



Mario Holzer, BSc

Differential pressure based wireless air flow sensor system for biomedical applications

MASTER'S THESIS

to achieve the university degree of

Diplom-Ingenieur

Master's degree programme: Biomedical Engineering

submitted to

Graz University of Technology

Supervisors:

Ao.Univ.-Prof. Dipl.-Ing. Dr.techn. Hermann Scharfetter
Institute of Biomedical Imaging
Stremayrgasse 16/III

Dipl.-Ing. Thomas Kammerhofer
Infineon Technologies Austria AG
Babenbergerstraße 10

Graz, June 2024

AFFIDAVIT

I - Mario Holzer - declare that I have authored this thesis independently, that I have not used other than the declared sources/resources, and that I have explicitly indicated all material which has been quoted either literally or by content from the sources used. The text document uploaded to TUGRAZonline is identical to the present master's thesis dissertation.

Date

Signature

Acknowledgement

First of all, I would like to thank my former manager Univ.-Prof. Dipl.-Ing. Dr.techn. Thomas Thurner for making the cooperation with Infineon Technologies even possible. I would also like to thank him for his enthusiasm and his constant motivating input in the course of this thesis. I would also like to thank Ao.Univ.-Prof. Dipl.-Ing. Dr.tech. Hermann Scharfetter for contributing his expertise and supervision.

Special thanks are due to my supervisor at Infineon Technologies and good friend Thomas Kammerhofer. His support and his always motivating words often helped me when I seemed to be stuck with problems. Thank you for your constructive criticism and helpful suggestions, which improved this work.

I would like to thank my parents Alexandra and Heinz Holzer for making all of this even possible by supporting me financially throughout my studies. I am so grateful that you are my parents and that I can always rely on you.

Finally, I would like to thank my wonderful girlfriend Birgit Eibel. You have always built me up and encouraged me after exhausting days. I am glad to have you in my life.

Kurzfassung

Die kabellose Verfügbarkeit verschiedener Sensordaten in sogenannten Sensornetzwerken bietet neue Möglichkeiten und Applikationen im Bereich Healthcare, Telemedizin und auch der Sportwissenschaft. Künstliche Intelligenz spielt bei der Auswertung von Biosignalen eine immer größere Rolle. Gleichzeitig kommen, vor allem in entlegenen Regionen, vermehrt telemedizinische Systeme zum Einsatz, um diagnostisch relevante Daten beim Patienten vor Ort aufzunehmen. Anschließend werden diese an einen Arzt übermittelt, woraufhin dieser diagnostische Schlüsse anhand der remote aufgenommenen Daten ziehen kann. Eine Schlüsselrolle spielt dabei die korrekte Erfassung der Signale, als auch die Übertragung der Daten unter möglichst geringem Energieverbrauch. In dieser Masterarbeit wird ein kabelloses Luftstrommesssystem zur Messung von Atemstrom und Atemvolumen unter Verwendung eines digitalen Differenzdrucksensors entwickelt. Der Atemstrom verursacht an einem Strömungswiderstand einen Differenzdruck. Sowohl der Differenzdruck, als auch die Temperatur werden von dem Differenzdrucksensor mit einer Bittiefe von 24 Bit und einer Abtastrate von 128 Hz digitalisiert. Der digitalisierte Differenzdruck wird mittels Bluetooth® Low Energy an eine Host Device übertragen und dort in Atemstrom umgerechnet. Aus diesem wird anschließend mittels numerischer Integration das Atemvolumen berechnet. Die Atemstrom- und Atemvolumenkurve werden anschließend grafisch dargestellt. Die Arbeit beinhaltet außerdem die Charakterisierung des verwendeten Strömungswiderstands. Hinsichtlich der Performance wurde das System mit einem state of the art Ultraschallspirometer verglichen und der Stromverbrauch des Systems untersucht und bewertet, sowie Maßnahmen zur weiteren Performanceverbesserung definiert.

Abstract

The wireless provision of various sensor data in so-called sensor networks offers new possibilities and applications in the fields of healthcare, telemedicine and sports science. Artificial intelligence is playing an increasingly important role in the analysis of biosignals. At the same time, telemedicine systems are increasingly being used, especially in remote regions, to record diagnostically relevant data from patients on site. This data is then transmitted to a doctor to make a diagnosis. A key role is played here by the correct recording of the signals, as well as the most energy-efficient transmission of the data. In this master's thesis, a wireless airflow measurement system for measuring respiratory flow and respiratory volume is being developed using a digital differential pressure sensor. The respiratory flow causes a differential pressure at a flow resistor. This differential pressure, as well as the temperature, is digitised by the differential pressure sensor with a bit depth of 24 bits and a sampling rate of 128 Hz. The digitised differential pressure is transferred to a computer using Bluetooth[®] Low Energy and converted into respiratory flow. The respiratory volume is then calculated from this using numerical integration. Both curves are then displayed graphically. The work also includes the characterisation of the flow resistance used. Furthermore, the system was compared with a state of the art ultrasonic spirometer and the power consumption of the system was analysed.

Contents

Contents	VII
List of Figures	X
List of Tables	XIII
1 Introduction	1
1.1 Motivation	1
1.2 Fundamentals	4
1.2.1 Human respiratory system	4
1.2.1.1 Physiology and Anatomy	4
1.2.1.2 Static lung volume	5
1.2.1.3 Dynamic lung volume	6
1.2.2 Spirometer	7
1.2.2.1 Principle	7
1.2.2.2 Requirements	8
1.2.3 The law of Hagen-Poiseuille	9
1.2.4 Bluetooth® Low Energy	10
1.2.4.1 Generic Access Profile	12
1.2.4.2 Generic Attribute Profile	13
1.2.5 Digital capacitive pressure sensors	14
1.2.6 Real time operating system	15
1.3 State of the art	17
1.3.1 Digital differential pressure sensors	17
1.3.1.1 Infineon digital differential pressure sensor . .	17
1.3.1.2 Sensirion SDP31	18
1.3.2 Flow meters	20

1.3.2.1	Differential pressure flow meter	20
1.3.2.2	Turbine flow meter	21
1.3.2.3	Ultrasound flow meter	21
1.3.3	Wireless Spirometers	22
1.3.3.1	Spirobank II Smart	22
1.3.3.2	EasyOne® Air Spirometer	23
1.3.3.3	SpiroSonic MOBILE	23
1.4	Aim of this thesis	23
2	Materials and Methods	25
2.1	Concept	25
2.2	Hardware	26
2.2.1	Electronic Components	26
2.2.1.1	Microcontroller Unit	26
2.2.1.2	Digital differential pressure sensor	28
2.2.2	Circuit Design	28
2.2.3	Circuit Manufacturing	29
2.2.4	3D Design	29
2.2.5	3D Printing	30
2.3	Spirometer V1	30
2.3.1	Flow element V1	31
2.3.2	Sensor PCB V1	32
2.4	Spirometer V2	33
2.4.1	Flow element V2	33
2.4.2	Sensor PCB V2	34
2.5	Characterization of Lilly mesh	35
2.5.1	Measurement setup	36
2.5.2	Fitting	37
2.6	Firmware	38
2.6.1	IDE and evaluation kit	38
2.6.2	Custom service and characteristic	38
2.6.3	Program Flow	40
2.7	Software	44
2.7.1	BLE server	44
2.7.2	MATLAB® Script	45
2.7.2.1	Connection with the Spirometer V2	45

2.7.2.2	Post processing	45
2.7.2.3	Calibration and BTPS correction	46
2.8	Module performance	47
2.8.1	Comparison to the ndd Easy on-PC spirometer	47
2.8.2	Charge consumption and estimated lifetime	48
3	Results	49
3.1	Lilly membrane characterisation	49
3.1.1	Measurement	49
3.1.2	Fitting	52
3.2	MATLAB® Script	54
3.2.1	Differential pressure measurement	54
3.2.2	Flow volume measurement	56
3.3	Performance of the IFX-Spirometer	56
3.3.1	Calibration	56
3.3.2	Comparison to Easy on PC	57
3.3.2.1	Exhalation	59
3.3.2.2	Inhalation	62
3.3.3	Charge consumption and lifetime	65
4	Discussion and Outlook	67
	Bibliography	69
A	Instruments and assembly equipment	73
B	Inventor	77
B.1	Flowelement V1	78
B.2	Flowelement V2	80
B.3	Pressure Chamber	82
C	Printed Circuit Boards	85
C.1	Sensor PCB V2	85

List of Figures

1.1	Anatomy of the human respiratory system[8]	4
1.2	Overview of the static lung volumes [9]	5
1.3	Standardized curves as outcome of the forced spirometry.	7
1.4	Laminar flow with velocity v in a cylindrical pipe of length l and radius r . p_1 and p_2 are the pressures within the pipe as illustrated. The flow is represented here with the velocity v . To obtain Q , the mean of v (\bar{v}) is divided by the area A of the pipe. [12]	9
1.5	BLE band and network topologies. [16]	11
1.6	Bluetooth [®] Low Energy stack [17]	12
1.7	DPS368 Digital XENSIV [™] barometric pressure sensor	14
1.8	Illustration of the sensor package with ASIC and MEMS of the DDPS.	17
1.9	Sensirion SDP31	19
1.10	Schematics of flow meters based on different principles.	20
1.11	Different wireless spirometers	22
2.1	Drawing of wireless air flow sensor concept	25
2.2	Drawing of the QFN-56 package in with the AIROC [™] CYW20829 comes. [29]	26
2.3	Block diagram of the CYW20829 with it's peripherals and sub systems. [30]	27
2.4	DDPS connected to the MCU via IIC with two pull up resistors and optional interrupt connection.	28
2.5	Spirometer V1 system. Part A is the flow element V1. Part B ist the sensor PCB V1.	30
2.6	3D printed parts of the flow element V1. Part A is the pipe through which the air flows. Part B is the screwed and glued pneumatic connector. Part C is the Lilly membrane (flow resistance).	31

2.7	Sensor PCB. Part A ist eh DDPS. Part B ist the DPS368. Part C ist the 3D printed chamber.	32
2.8	SpirometerV2. Part A is the flow element, Part B the sensor PCB, Part C the bacteria filter for spirometry.	33
2.9	Design of the Sensor PCB V2. Part A is the DDPS. Part B is the antenna path. Parts C are the two external crystal oscillators. Part D is the external QSPI flash. Part E ist the AIROC™ CYW20829. .	34
2.10	Picture of the populated sensor PCB V2	35
2.11	Image of the measurement setup. Part A is the wind tunnel. Part B the Easy on-PC spirometer. Part C ist the spirometer system V1. Part D is a interface PCB. Part E is a NI USB-8452 IIC/SPI interface.	36
2.12	AIROC™ CYW20829 Bluetooth® LE SoC evaluation kit (Part B) connected with the sensor PCB V1 (Part C). Part B is the module with the micro controller and all required peripheral components and also the antenna.	39
2.13	Bluetooth® Configurator 2.5 with the GATT database visible on the left column with the selected custom characteristic Pressure and Temperature. The right column shows the properties of the custom characteristic.	40
2.14	Event 1 - query of the state of the connection	41
2.15	Event 2 - query of the state of the interrupt.	41
2.16	Main program flow of the developed firmware running on the AIROC™ CYW20829	43
2.17	Sketch of the signal chain using the BLE server	44
2.18	Example of the numerical integration of a sinus using trapezoidal method[35].	45
2.19	BTPS correction factors determined by the ndd Easy on-PC spirometer, read out with the WBreath software.	48
3.1	Relationship between applied flow Q and measured differential pressure Δp with 100 samples Δp per point Q	50
3.2	Statistical evaluation of the measurement results from the characterization of the Lilly membrane	51
3.3	Identified model of the flow resistor	52
3.4	Data and fit which describes the relationship between Flow Q and differential pressure Δp	53

3.5	Differential pressure measured with the IFX-Spirometer without using a breathing filter	55
3.6	Differential pressure measured with the IFX-Spirometer using a breathing filter	55
3.7	Flow and volume measured with the IFX-Spirometer. The blue curve is the air flow. The orange curve is the volume.	56
3.8	Flow of a complete exhalation measured using IFX-Spirometer (red curve) and US-Spirometer (blue curve)	59
3.9	Volume of a complete exhalation measured using IFX-Spirometer (red curve) and US-Spirometer (blue curve)	59
3.10	Comparison of determined Flow between IFX-Spirometer and US-Spirometer	60
3.11	Comparison of determined volume between IFX-Spirometer and US-Spirometer	61
3.12	Flow of a complete inhalation measured using IFX-Spirometer (red curve) and US spirometer (blue curve)	62
3.13	Flow of a complete inhalation measured using IFX-Spirometer (red curve) and US spirometer (blue curve)	62
3.14	Comparison of determined volume between IFX-Spirometer and US-Spirometer	63
3.15	Comparison of determined volume between IFX-Spirometer and US-Spirometer	64
3.16	Screen capture of the current waveform analyzer used for the charge consumption measurement.	65
C.1	Top layer of the Sensor PCB V2	85
C.2	Layer 2 of the Sensor PCB V2	86
C.3	Layer 3 of the Sensor PCB V2	86
C.4	Bottom layer of the Sensor PCB V2	87

List of Tables

1.1	Parameters of forced spirometry and what they mean.	6
1.2	Tradeoff between oversampling rate (OSR) and sampling frequency (f_s) for the DDPS	18
3.1	Result of three calibration runs performed with a 2l syringe. . . .	57
A.1	Used equipment for assembly and testing	74
A.2	List of materials necessary for assembling a single module V1.0 . .	75

Acronyms

ADC analog-digital converter.

ASIC application-specific integrated circuit.

ATP Ambient Temperature and Pressure.

ATT attribute protocol.

BLE Bluetooth[®] Low Energy.

BT Bluetooth[®].

BTPS Body Temperature and Pressure, Saturated.

COPD chronic obstructive pulmonary disease.

ENIG Electroless Nickel Immersion Gold.

ERV expiratory reserve volume.

FEV₁ forced expiratory volume after 1s.

FEV₃ forced expiratory volume after 3s.

FHSS frequency-hopping spread spectrum.

FIVC forced inspiratory vital capacity.

FRC functional residual capacity.

FVC forced expiratory vital capacity.

- GAP** Generic Access Profile.
- GATT** Generic Attribute Profile.
- GFSK** gaussian frequency shift keying.
- GND** ground.
- GPIO** general purpouse input output.
- GUI** grafical user interface.
- HCI** host controller interface.
- IDE** integrated development environment.
- IFX** Infineon Technologies AG.
- IIC** inter-integrated circuit.
- IoT** internet of things.
- IRV** inspiratory reserve volume.
- ISM** Industrial-Scientifical-Medical.
- ISR** interrupt service routine.
- L2CAP** logical link control and adaption protocol.
- LCD** liquid crystal display.
- MCU** micro controller unit.
- MEMS** micro-electro-mechanical system.
- PC** personal computer.
- PCB** printed circuit board.
- PHY** physical layer.
- QSPI** quad serial peripheral interface.

RTOS real time operating system.

RV residual volume.

SIG Special Interest Group.

SoC System on Chip.

SPI serial peripheral interface.

ToF time of flight.

TUG Technical University of Graz.

TV tital volume.

UART universal asynchronous receiver transmitter.

USB universal serial bus.

UUID Universally Unique Identifier.

VC vital capacity.

CHAPTER 1

Introduction

This master's thesis was created in collaboration with Infineon Technologies AG (Design Centre Graz).

1.1 Motivation

Due to the further development of technology, integrated circuits in particular are becoming smaller, more efficient and more powerful. This effect is described by Moore's Law, which states that the number of transistors in integrated circuits doubles approximately every two years[1]. This has led to an increase in high-performance, battery-powered devices, especially in recent years. The best known of these is probably the smartphone, which also provides access to the internet via the mobile data network. However, smaller devices, which also had access to the internet wireless directly or in combination with wireless communication to a smartphone, also quickly became established. These devices are referred to as internet of things (IoT)[2] devices. The manufacturers of such IoT devices began to equip them with all kinds of sensors. As a result, smartwatches became personal health trackers in which the heart rate, blood pressure, temperature, steps taken and the quality of sleep can be recorded by the smartwatch and later displayed and analyzed directly on the smartwatch itself or on the smartphone. At this point, however, it must be mentioned that this example concerns sports and lifestyle products and not medical devices.

These trends of combining sensors and wireless communication have also quickly found their way into the healthcare sector. A prominent example of this is the eversense® glucose sensor[3] from Ascensia Diabetes Care Holdings AG, which can be worn for several months and sends glucose values in real time to the smartphone every 5 minutes via Bluetooth®. People suffering from diabetes can therefore easily monitor their glucose levels and no longer need to prick their fingertips several times a day, which means a significant improvement in the quality of life.

Infineon Technologies AG (IFX) manufactures pressure sensors that have been developed for portable devices and IoT applications. This means that these sensors are comparatively very small, have very low energy consumption, are very accurate and are equipped with a digital interface. Furthermore, IFX is also represented in the wireless connectivity sector with its AIROC™ System on Chip (SoC) products which have WiFi or/and Bluetooth® Low Energy (BLE) communication interfaces. The combination of such a micro controller unit (MCU) with one or more pressure sensors offers the possibility to build an easy to integrate, wireless airflow sensor module for measuring lung or respiratory volume. These can then be used in the field of spirometry or as sensor in ventilator systems. Equipped with additional sensors such as a CO₂ sensor and an O₂ sensor, such a device can also be interesting for performance diagnostics in the form of a small portable ergospirometer.

In the field of telemedicine, IoT-devices offer a completely new type of interaction between doctor and patient. For example in emergency medicine, it is already possible to forward all diagnostic parameters (ECG, SpO₂, blood pressure, blood sugar, temperature) collected by the emergency services directly from the monitoring system to a tele-emergency doctor. The tele-emergency doctor can use this information and communication with the patient via video chat to assess the medical situation and initiate further steps if necessary. This system is already in use today, particularly in remote regions, and has proven its worth in relieving the burden on medical facilities.[4] With a BLE-spirometer, which transmits data wirelessly to a host device, the same principle can be applied to lung function diagnostics. This means that

people suffering from chronic obstructive pulmonary disease (COPD) who find it difficult to visit the doctor can undergo their regular check-up at home and save themselves the trouble of visiting a lung specialist.

In February 2020, Italy was the first European country to face a rapid exponential increase in SARS-Cov-2 infections. This also led to such an increase in hospitalisations in intensive care units, resulting in a shortage of ventilators.[5] Several initiatives, which are summarised in [6], were quickly launched for a so-called OpenVentilator. This is an alternative open source ventilation system. As measuring the administered volume is very important for ventilation systems, an accurate, easy-to-integrate flow sensor is required here.

1.2 Fundamentals

This section is intended to give the reader an overview of the theoretical foundations that are a prerequisite for understanding the realisation of this Master's thesis.

1.2.1 Human respiratory system

The following section describes the structure of the lungs and the function of respiration, as well as the static and dynamic lung volumes.

1.2.1.1 Physiology and Anatomy

Through the respiratory system, the body is exchanging gases with the environment. Oxygen (O_2) is taken from the air for the oxidative processes of the cell metabolism, while the so produced carbon dioxide (CO_2) is released. The gases are transported via the blood between tissue and lung. The gas exchange happens in the lung in the alviols.[7]

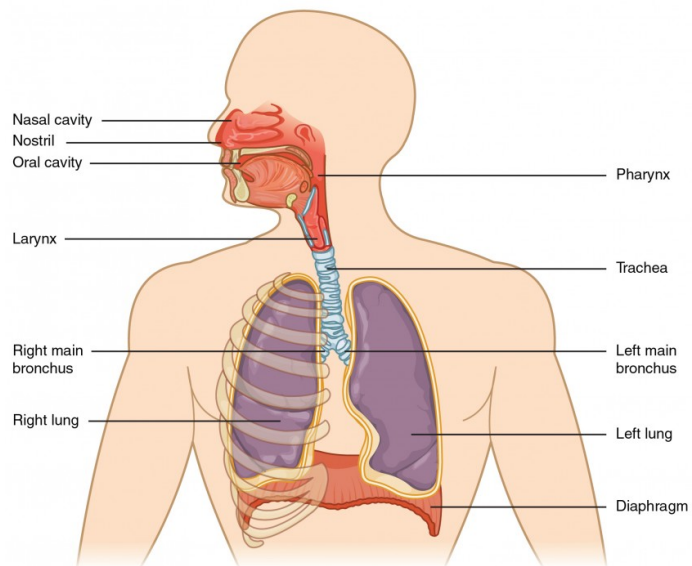


Figure 1.1: Anatomy of the human respiratory system[8]

The anatomy of the respiratory system is subdivided in upper and lower airway. The nose, nose cavity and the mouth are part of the upper airway. The

larynx, trachea, bronchia and the lung are part of the lower airway. To inhale, the lungs are stretched by raising the thorax and lowering the diaphragm. This creates a negative pressure in the lungs, relative to the environmental pressure, and air flows into the lungs via the airways. This phase is called inspiration. To exhale, the thorax and diaphragm are relaxing so that the lung can take it's initial position. The air streams out of the lung. This phase is called expiration. While the inspiration is an active process, the expiration happens mostly passive, but can also be actively increased to further deflate the lungs.[7]

1.2.1.2 Static lung volume

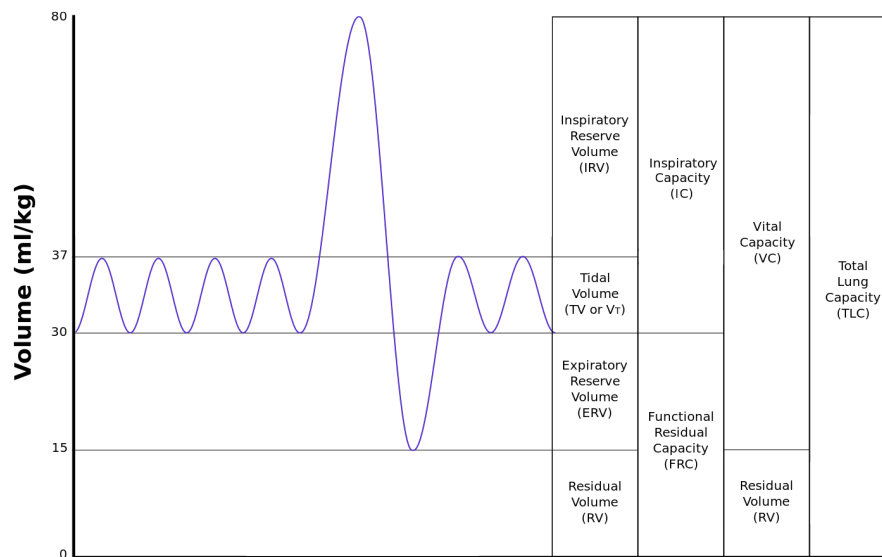


Figure 1.2: Overview of the static lung volumes [9]

The volume that is inhaled or exhaled during a normal breath is referred to as tidal volume (TV). The average tidal volume (TV) of an adult human is 0.5l. If one now inhale and exhale to the maximum, this is called the inspiratory reserve volume (IRV) and expiratory reserve volume (ERV). The IRV for an average adult is 3l and the ERV is 1.7l. These three volumes are added up to the so called vital capacity (VC). This is the maximum volume that

can be inhaled and exhaled by a healthy adult. After maximum exhalation, some volume remains in the lungs, which is referred to as residual volume (RV). The RV for an average adult is 1.3l and cannot be determined using a lung function test. RV and ERV are summarized as functional residual capacity (FRC). [7] These lung volumes are static volumes that result from the anatomy of the lungs.

1.2.1.3 Dynamic lung volume

The dynamic lung volumes are of particular diagnostic relevance. These are determined during so-called forced spirometry. During this test, the subject is encouraged to perform maximum inspiration and expiration. The forced expiratory vital capacity (FVC) and the forced expiratory volume after 1s (FEV_1), shown in Figure 1.2 and Figure 1.3a, are part of the basic diagnostics. Probably the most important diagram for diagnostics is the flow-volume diagram. Figure 1.3b shows the diagram of a healthy average person. It provides a quick overview of the function of the lungs and any pathologies. All other important dynamic parameters are listed in the following Table 1.1. The so called Tiffeneau-index is gold standard for diagnosing COPD.[10]

Parameter [Dimension]	Discription
$FVC[l]$	forced expiratory capacity
$FIVC[l]$	forced inspiratory vital capacity
$FEV_1[l]$	forced expiratory volume after 1s
$FEV_3[l]$	forced expiratory volume after 3s
$FEV_1/FVC[\%]$	Tiffeneau-index
$FEF_{25-75}[l/s]$	Maximum mid-expiratory flow
$FEF_{25}[l/s]$	expiratory flow at 25% VC
$FEF_{50}[l/s]$	expiratory flow at 50% VC
$FEF_{75}[l/s]$	expiratory flow at 75% VC
$FIF_{50}[l/s]$	inspiratory flow at 50% VC
$PEF[l/s]$	peak expiratory flow
$FET[s]$	forced expiratory time

Table 1.1: Parameters of forced spirometry and what they mean.

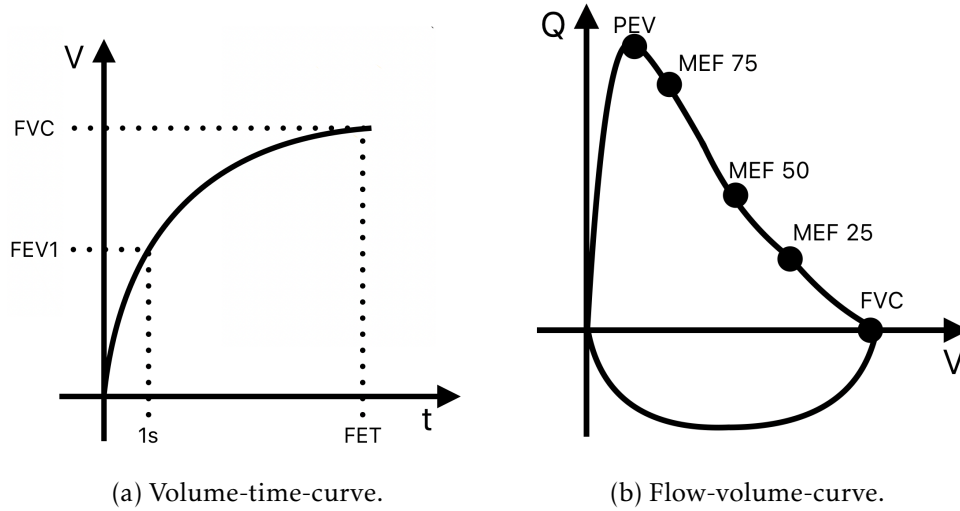


Figure 1.3: Standardized curves as outcome of the forced spirometry.

1.2.2 Spirometer

This section deals with the general technical principles of spirometry as well as the physical principles of differential pressure-based airflow measurement.

1.2.2.1 Principle

A Spirometer is a non-invasive diagnostic tool, which is used to investigate lung parameters. Three main parameters are determined by spirometry:

1. Flow rate $Q[\frac{l}{s}]$ (often also referred to as $\dot{V}[\frac{l}{s}]$)
2. Time $t[s]$
3. Lung volume $V[l]$

The basic measurement principle is nearly the same for all types of spirometers. The patient is breathing into a vessel. A certain type of flow sensor is measuring $Q(t)$ within the vessel. Time t is also measured by the spirometer system. The volume V is determined via integration of $Q(t)$ over t , as given in equation 1.1.

$$V = \int_{t_1}^{t_2} Q(t) \cdot dt \quad (1.1)$$

The determined parameters are then displayed standardized as volume-time-curve and flow-volume-curve. Figure 1.3 is showing typical curves. Medical professionals are using these curves to get an impression of the patients respiratory system and to state a diagnosis.

1.2.2.2 Requirements

To enable correct measurement of the respiratory flow, certain requirements must be met by the flow sensor. The resolution should be $10 \frac{\text{ml}}{\text{s}}$. A maximum flow of $16 \frac{\text{l}}{\text{s}}$ must be able to be recorded bidirectionally. This results in a dynamic range of 20l with a resolution of 500ppm. Due to the slow rate of the flow signal, a linear frequency response up to at least 15Hz is required. Therefore the sampling rate should be at least 30Hz. However, modern systems are sampling with a sampling rate between 100Hz and 400Hz. The dead space of the sensor should not exceed 35ml. For hygienic reasons, a special bacteria filter or a disposable tube should also be used to prevent cross-contamination between patients. The flow resistance, which is described in more detail in the following chapter, of the breathing filter and the spirometer should not exceed $1.5 \frac{\text{hPa}\cdot\text{s}}{\text{l}}$. [10]

Another requirement for the spirometer is the calibration. This is carried out using a calibration pump, which delivers a defined volume. The volume determined by the spirometer must correspond to the defined volume of the pump. Most spirometers have a calibration routine in which several pump strokes are recorded and averaged by the spirometer. Using the deviation from the defined value, a corresponding calibration factor can be determined and then used to correct the measured values. [10]

Another important point to note in spirometry is the conversion from Ambient Temperature and Pressure (ATP) conditions to Body Temperature and Pressure, Saturated (BTPS) conditions; i.e. 37°C, ambient pressure, 100% humidity. At ATP, 1l of ambient air corresponds to approximately 1.1l of lung air at BTPS. All measured parameters in spirometry are given in BTPS conditions. The exact conversion factor depends on the design and the sensor principle used within the spirometer and must therefore be verified experimentally. [10] However, an estimate can be made for the inspiratory BTPS

factor $BTPS_{in}$ using the following analytical formula:

$$BTPS_{in} = \frac{T_{body}}{T_{amb}} \cdot \frac{p_{amb} - p_{H_2O}(T_{amb}, H_{amb})}{p_{amb} - p_{H_2O}(T_{body}, H_{body})} \quad (1.2)$$

With T for temperature, p for pressure, $p_{(H_2O)}$ for water vapour partial pressure, which in turn depends on the temperature and relative humidity. Sensors for absolute air pressure, ambient temperature and humidity are installed in modern spirometers to ensure correct estimation. The temperature difference between the air in the lungs and the air at the sensor is taken into account for the expiratory BTPS factor $BTPS_{ex}$. This depends on the design of the spirometer and must be determined experimentally. However, to test whether a spirometer meets all these requirements, 24 so-called standard waveforms were introduced in [11]. These cover the entire physiological and pathological signal range [10]. They are emitted by a computer-controlled mechanical pump system. The BTPS conditions can also be set to implement an sufficient algorithm for BTPS correction or to verifying one.[11]

1.2.3 The law of Hagen-Poiseuille

A non-ideal¹ liquid or a non-ideal gas with constant viscosity η flows through a cylindrical pipe with radius r and length l at a certain flow rate Q . Pressure p_1 prevails at the beginning of the pipe and pressure p_2 at the end of the pipe. The pipe is illustrated in the following Figure 1.4.

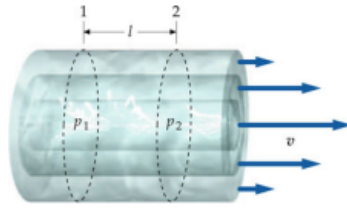


Figure 1.4: Laminar flow with velocity v in a cylindrical pipe of length l and radius r . p_1 and p_2 are the pressures within the pipe as illustrated. The flow is represented here with the velocity v . To obtain Q , the mean of v (\bar{v}) is divided by the area A of the pipe. [12]

¹In an ideal medium, friction is neglected.

Since the medium is non-ideal, the friction of the flowing medium on the wall of the pipe and the friction between the particles of the medium result in a pressure difference Δp . If the flow in the pipe is laminar, the pressure drop Δp is proportional to the volume flow Q and can be described as follows:

$$\Delta p = p_1 - p_2 = R \cdot Q \quad (1.3)$$

Where R is referred to as flow resistance and results from the geometry of the pipe and the viscosity of the flowing medium as follows:

$$R = \frac{8 \cdot \eta \cdot l}{\pi \cdot r^4} \quad (1.4)$$

If equation 1.4 is now inserted into equation 1.3, the law of Hagen-Poiseuille is obtained:

$$\Delta p = \frac{8 \cdot \eta \cdot l}{\pi \cdot r^4} \cdot Q \quad (1.5)$$

As mentioned, the prerequisite for the validity of this law is a laminar flow in the pipe. The calculation of the Reynolds number can be used to estimate whether a laminar flow is present or not. Whether a flow becomes turbulent depends on the radius r of the tube, the density ρ , the viscosity η and the mean velocity v of the flowing medium:

$$Re = \frac{2 \cdot r \cdot \rho \cdot v}{\eta} \quad (1.6)$$

Flows with $Re < 2000$ are mostly laminar, while flows with $Re > 3000$ are mostly turbulent. As other factors such as the surface of the tube also have an influence on the flow, there is an unstable area in the range of $2000 \leq Re \leq 3000$ in which the flow can change from one type to the other. In this case, it must be determined experimentally whether laminar flow is present or not. [12]

The law of Hagen-Poiseuille is the foundation for some differential pressure-based spirometers such as the spirometer according to Fleisch or the spirometer according to Lilly.

1.2.4 Bluetooth® Low Energy

Bluetooth® Low Energy (BLE) was introduced in 2010 within the Bluetooth® 4.0 core specifications by the Bluetooth® Special Interest Group (SIG), Inc.

[13]. The previous standard was known as Bluetooth® Classic and was designed to provide wireless connectivity between mobile phones and other portable devices[14]. Although some protocols have been adopted from Bluetooth® Classic, BLE is a completely different technology for other design goals and other applications[15]. It was specially developed as a more efficient and less complex alternative to Bluetooth® Classic for use in the area of IoT and beyond [14][15].



(a) 2.4GHz ISM band with the 2MHz broad channels. The advertising channels are displayed in a darker gray than the data channels.



(b) Network topologies that are supported by BLE.

Figure 1.5: BLE band and network topologies. [16]

BLE operates in the 2.4GHz (2.402–2.480GHz) Industrial-Scientific-Medical (ISM) band. The band is divided into 40 channels with 2MHz spacing (Figure 1.5a). Three of these channels are used so that devices can recognize each other, communicate their role and establish connections. This is known as advertising. The remaining 37 channels are used as data channels. The data channels are used via frequency-hopping spread spectrum (FHSS), which is intended to prevent collision of data packets. The data is modulated using gaussian frequency shift keying (GFSK).[16] Communication can either be connection less using broadcasting, connection-orientated using point-to-point connection or in a mesh network (Figure 1.5b). BLE also has position-

determining properties with which distances between the devices and also directions to other devices can be determined.[16]

With BLE, unlike Bluetooth[®] Classic, a connection is not maintained continuously. Instead, data packets are exchanged at a specific interval, the so called connection interval. The connection interval is defined before a connection is established and can be between 7.5ms and 4s[16]. As no communication is required between the connection intervals, the radio is switched off during this period to save energy.

The BLE protocol is broken down into smaller protocols, which are packaged into a layered architecture called the BLE stack [17]. The BLE stack is shown in Figure 1.6. Only the top three layers are important for the development of BLE applications, which are therefore described in more detail below. Information about all layers of the BLE stack can be found in [17].

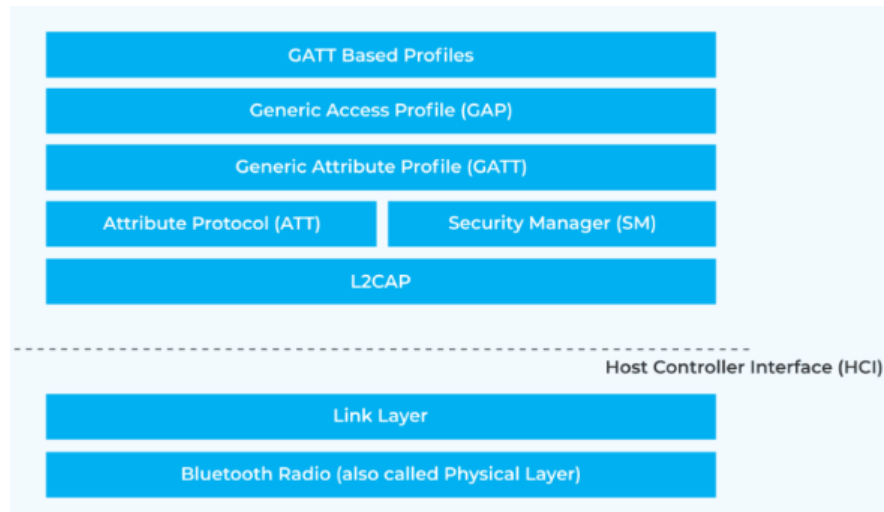


Figure 1.6: Bluetooth[®] Low Energy stack [17]

1.2.4.1 Generic Access Profile

The Generic Access Profile (GAP) defines how a BLE device interacts with another. This includes the role of a device, which can be broadcaster, observer, central or peripheral. As a broadcaster, a device is only sending out

advertisement packages. It is not receiving data or is allowing a connection. As observer, a device is only listening to advertisement packages and is not allowing a connection. A central device is listening to advertising devices and can also connect to one. A peripheral device is advertising and is accepting connection requests from a central device. The GAP is also managing the advertisements. This includes broadcasting, discovery, advertisement parameters and advertisement data. Connection establishment is also something that is managed by GAP. This includes initiation of connections, accepting connections and exchange of connection parameters like connection interval and the hop increment to change between the data channels with FHSS.[17][13]

1.2.4.2 Generic Attribute Profile

The Generic Attribute Profile (GATT) defines the data exposed by BLE devices. Devices can have two roles within GATT: Server and Client. The server exposes data, which can be controlled by the server itself or by the connected client. The client interfaces with the server by reading the data exposed by the server and/or controlling the servers behavior. A device can also act as server and client simultaneously.[17]

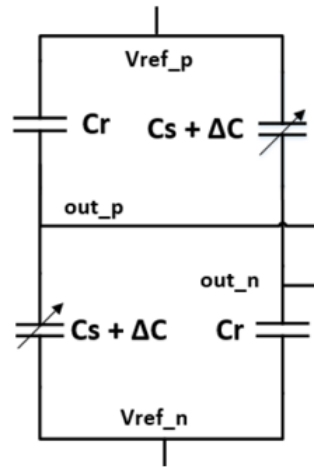
The data within GATT is subdivided into services and characteristics. A service is a group of any type of data exposed by the server. It's purpose is, to group together related data types to satisfy a specific functionality on the server. A characteristic is always part of a service, representing a piece of data the server wants to expose to a client.[17] Each service and each characteristic has it's unique and identifiable Universally Unique Identifier (UUID) which is a 16 bits or 128 bits long number. The UUIDs are registered by the Bluetooth® SIG [18]. With this numbers it is possible to identify the provided data between BLE devices.

The advantage of BLE is that such services and characteristics can be created very easily as so-called **custom services** and **custom characteristics**. The data type and length can be defined as required within the Bluetooth® core specifications and adapted to the specific use case. The UUID for custom services and custom characteristics should not correspond to already registered UUIDs. There is no need to register custom services and custom characteris-

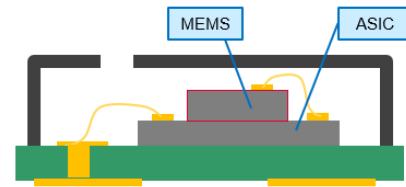
tics at the Bluetooth® SIG. This is only necessary if one want to establish it's services and characteristics as standard. As these are tailored to the sensor used in this case, this would not be expedient.

1.2.5 Digital capacitive pressure sensors

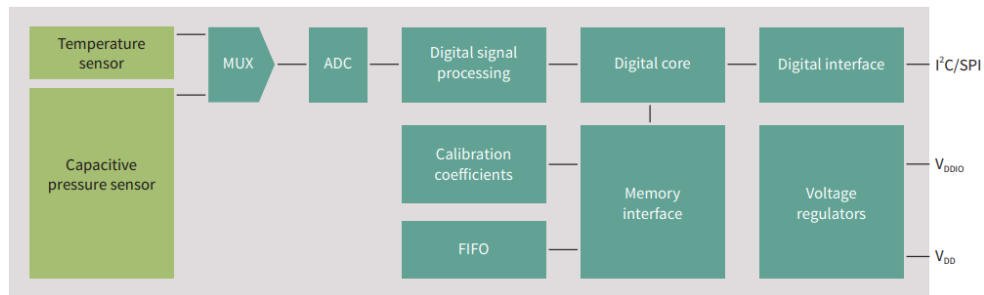
This chapter discusses the general design of digital capacitive pressure sensors using the DPS368 Digital XENSIV™ barometric pressure sensor, which is an absolute pressure sensor in operating range 300 – 1200hPa. Capaci-



(a) Schematic representation of the capacitive bridge circuit.[19]



(b) Illustration of the sensor package with ASIC and MEMS bonded together and to the connection contacts on the substrate.[19]



(c) Blockdiagram with all functional blocks and connections.[20]

Figure 1.7: DPS368 Digital XENSIV™ barometric pressure sensor

tive sensors are constructed from membranes that deform when the ambient pressure changes. This deformation results in a change in capacitance. Two membranes that are exposed to the change in pressure are connected together in a bridge with two other membranes that are not exposed to a change in pressure. The bridge circuit (Figure 1.7a) with two active and two reference capacitance increases the sensitivity and reduces the temperature dependence.[19] The membranes, interconnected in the bridge, are subsequently referred to as micro-electro-mechanical system (MEMS). If there is a change in pressure, the membrane deforms and the value of the capacitance changes as a result. This in turn leads to a change of the electrical parameters of the bridge. The bridge is supplied by an application-specific integrated circuit (ASIC). The ASIC also contains all the other components of a typical measurement chain, such as the amplifier, the analog-digital converter (ADC), digital signal processing and data storage. It also provides the digital interfaces such as inter-integrated circuit (IIC) and serial peripheral interface (SPI). The sensor can be configured via these interfaces. The configuration is stored in volatile memories (registers) as long as the ASIC is supplied sufficiently. If no measurement is being carried out, the MEMS and all other blocks that are not required are not supplied. The sensor is then in "standby mode" and has a lower energy consumption. This is a huge advantage over analogue sensors when it comes to energy efficiency. It must be mentioned here that the sensor used in the practical part of this work is a different one, but the sensing principle and the ASIC of the used sensor are the same as described above. The structure of the MEMS within the used sensor is designed for differential pressure.

1.2.6 Real time operating system

A real time operating system (RTOS) is a concept which is used to reduce complexity of developing embedded firmware where the developer has to deal with asynchronous, response-time-critical tasks which are using overlapping resources. It ensures that timing requirements and support of peripherals are not causing any errors or collisions. For example maintaining a BLE connection while reading values from a peripheral sensor via IIC whenever the data is ready, can cause a collision, if both events are triggered at the same time. By using an RTOS, system functions can be separated into so

called threads or tasks. The so called scheduler is managing the tasks based on a list, which contains the current status of all tasks. The status of a task can be idle, halted or running. The list also contains which task will be executed next, based on priority. Event flags are signals within tasks, which are used to indicate a certain status. A task can then take appropriate action based on the value of an event flag. Once the event has been processed, the event flag can be cleared. Another important functionality are interrupts. An interrupt is a signal to the processor, that an event has occurred, which needs immediate attention. Interrupts are not a RTOS specific function, but they are interacting with RTOS. The so called interrupt service routine (ISR) is responsible for handling an interrupt. An ISR is a function, which should ideally be as short as possible to take up as little time as possible. In most cases, only event flags are set in an ISR, which subsequently signal a task to execute a certain routine. In RTOS interrupts also have priorities. This can cause an ISR for a lower priority interrupt to suspend until the higher priority ISR is completed.[21]

1.3 State of the art

This section discusses the state of the art methods for differential pressure sensors, flowmeters and wireless spirometers.

1.3.1 Digital differential pressure sensors

In the following, two digital differential pressure sensors with different sensing principles are compared.

1.3.1.1 Infineon digital differential pressure sensor

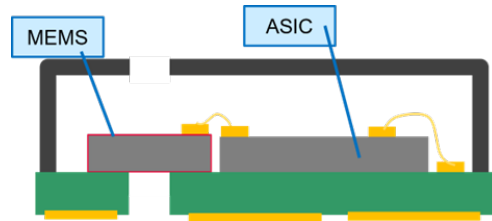


Figure 1.8: Illustration of the sensor package with ASIC and MEMS of the DDPS.

The Infineon digital differential pressure sensor (subsequently referred to as DDPS) is still under development and is not available commercially. Similar to the DPS368 presented in section 1.2.5, it has an ASIC and a special capacitive MEMS developed for differential pressure. The package has an opening on the top and on the bottom. The MEMS deforms according to the pressure difference between the upper and lower opening. It also has an integrated temperature sensor. The $\Sigma\Delta$ -ADC of the sensor provides the temperature and pressure values in 24-Bit results. Calibration coefficients are also stored in the sensor. These are combined with the raw 24-Bit pressure and temperature values in a polynomial equation (see Equation 1.7) to obtain a temperature compensated differential pressure value. Communication with the sensor takes place via IIC or SPI. When using IIC, a pin can also be used to trigger an interrupt signal as soon as a result is ready to be read out, thus ensuring efficient readout. The sampling frequency and precision (oversampling) can also be configured. The maximum sampling frequency of the sensor is 128 Hz. However, only low oversampling is possible

at maximum sampling frequency and vice versa. All possible combinations are listed in table 1.2. Due to the low current consumption of the DDPS, it is ideal for battery powered IoT applications. For a pressure measurement, the peak current consumption is $345 \mu\text{A}^1$, for a temperature measurement $280 \mu\text{A}^1$. In background mode the sensor consumes $0.5 \mu\text{A}^1$. The measuring range of the DDPS is between -500 Pa and 500 Pa with a zero point accuracy of 0.5 Pa and a span accuracy of 2.5% .

$f_s[\text{Hz}] \backslash \text{OSR}[1]$	1	2	4	8	16	32	64	128
1	✓	✓	✓	✓	✓	✓	✓	✓
2	✓	✓	✓	✓	✓	✓	✓	✓
4	✓	✓	✓	✓	✓	✓	✗	✗
8	✓	✓	✓	✓	✓	✓	✗	✗
16	✓	✓	✓	✓	✓	✗	✗	✗
32	✓	✓	✓	✓	✗	✗	✗	✗
64	✓	✓	✓	✗	✗	✗	✗	✗
128	✓	✓	✗	✗	✗	✗	✗	✗

Table 1.2: Tradeoff between oversampling rate (OSR) and sampling frequency (f_s) for the DDPS

The following equation is used to convert the raw temperature (T_{raw}) and the raw differential pressure (Δp_{raw}) into a compensated differential pressure (Δp) using the coefficients (c_i).

$$\Delta p = c_{00} + c_{10} \cdot \Delta p_{\text{raw}} + c_{20} \cdot \Delta p_{\text{raw}}^2 + c_{30} \cdot \Delta p_{\text{raw}}^3 + \dots + c_{01} \cdot T_{\text{raw}} + c_{11} \cdot T_{\text{raw}} \cdot \Delta p_{\text{raw}} + c_{21} \cdot T_{\text{raw}} \cdot \Delta p_{\text{raw}}^2 \quad (1.7)$$

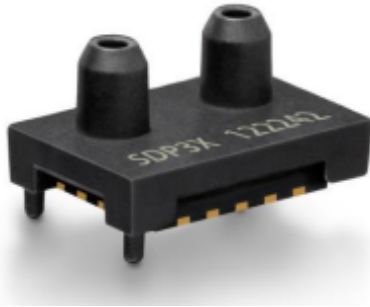
The coefficients are different for each individual sensor and are determined in a calibration procedure.

1.3.1.2 Sensirion SDP31

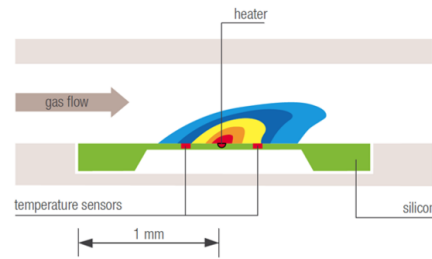
The Sensirion SDP31 is a digital differential pressure sensor manufactured by the Swiss company Sensirion AG. It comes in a small package, shown in

¹For a supply voltage of $V = 1.8 \text{ V}$ and ambient temperature of $T_A = 25^\circ\text{C}$

Figure 1.9a, that is suitable for portable applications. In addition to the differential pressure, it also equipped with a temperature sensor. It is calibrated for Air and Nitrogen and can compensate for the effects of temperature fluctuations in a range of -40°C to 85°C . It is also compatible with air, oxygen, nitrogen and non-condensing media. It can be operated in a continuous or triggered mode. The sensor is interfaced with IIC and has an interrupt pin which is triggered as soon as a measured value can be read out. The sensing principle is based on thermal conductivity through the gas flowing over the sensor surface [22], as illustrated in Figure 1.9b.



(a) Illustration of the package of the SDP31.



(b) Illustration of the measurement principle of the SDP31.

Figure 1.9: Sensirion SDP31

The measuring range of the SDP31 is between -500 Pa and 500 Pa . The zero point accuracy is 0.1 Pa while the span accuracy is 3% of the measured differential pressure. The differential pressure and temperature are digitised by a 16 bit ADC and is sampled at fixed sampling frequency between 1800 Hz and 2200 Hz (typically 2000 Hz) in continuous mode. The sensor also has an averaging function in continuous mode. If this is activated, the measured values are averaged until they are read out. If this is not activated, the value in the register is simply updated. The supply voltage can be between 2.7 V and 5.5 V . During a measurement, the current consumption is between 3.8 mA and 5.5 mA . [23]

1.3.2 Flow meters

The flow meters listed below are the most common when it comes to measuring respiratory gases, i.e. in the medical field. There are other methods that are not or no longer used in the medical field due to their complexity, inaccuracy or unreliability. These can be found in [7].

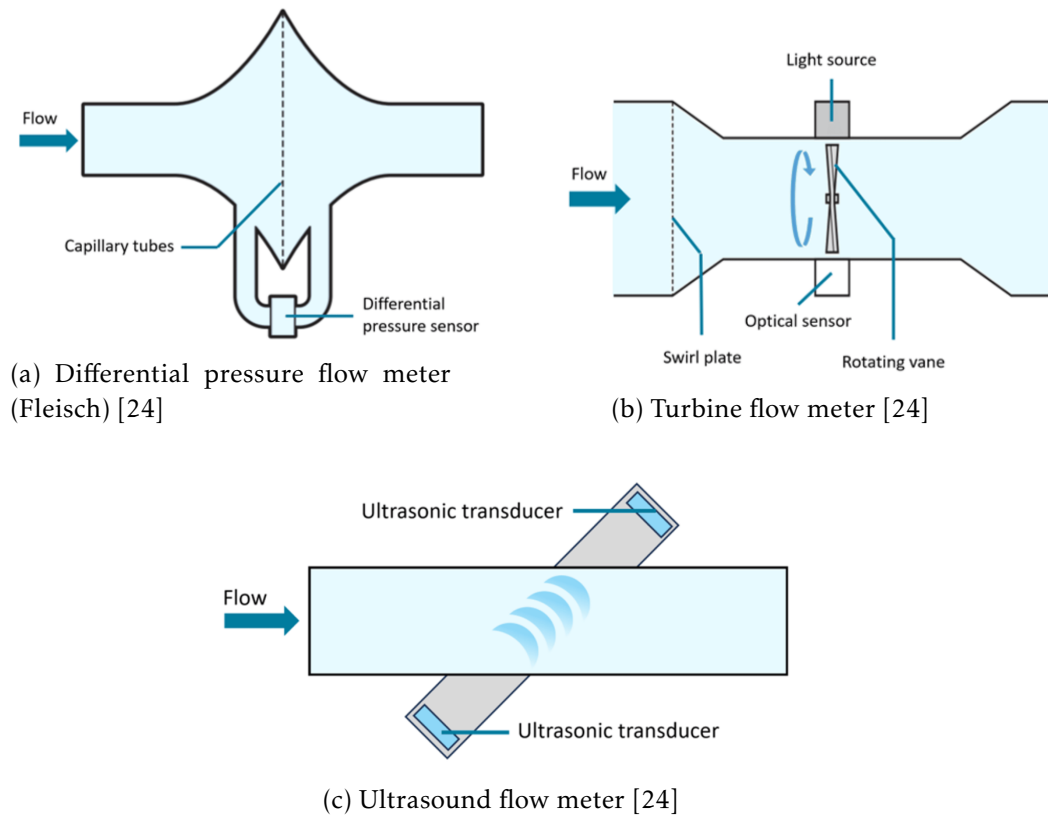


Figure 1.10: Schematics of flow meters based on different principles.

1.3.2.1 Differential pressure flow meter

In a differential pressure flowmeter, the air flow in a pipe causes a pressure drop at a flow resistor. The differential pressure is converted into an electrical signal by a transducer and then digitised. The relationship between flow and differential pressure is defined by the resistance and can be both linear and non-linear. These systems must be calibrated before use due to

the changed ambient conditions (absolute air pressure, temperature and humidity).

Looking at the concept of the pneumotachograph according to Fleisch, several capillary tubes are combined to form a bundle. The flow must be distributed over individual capillaries and is laminar in these. Each individual capillary forms a flow resistance. The number of capillary tubes arranged in parallel has an influence on the linearity and is determined so that the law of Hagen-Poiseulle (see equation 1.5) is valid.

In the pneumotachograph concept according to Lilly, a close-meshed net is used as a resistor. With this principle, each opening can also be regarded as an independent flow resistance. The flow is distributed evenly across all openings in the mesh, resulting in a linear relationship between flow and measured differential pressure over wide flow ranges in accordance with the law of **Hagen-Poiseulle** (see equation 1.5).

1.3.2.2 Turbine flow meter

In a turbine flow meter, a turbine is integrated in the centre of the flow path. This is caused to rotate by the breathing current and interrupts or reflects the light from one or more light beams. These are registered by photodiodes and convert these light pulses into electrical pulses. The frequency of these pulses is proportional to the velocity of the gas. The total number of pulses in a time frame is in turn proportional to the volume that flows through the turbine during that period.

1.3.2.3 Ultrasound flow meter

The principle of the ultrasonic flow meter is based on time of flight (ToF). The propagation speed of an acoustic wave is changed by the component of the flow vector in the direction of the sound transmission path. The ultrasonic waves are alternately emitted by the two ultrasonic transducers facing each other and received by the other. The flow velocity of the gas is calculated using the transit times determined. The dependence on the speed of sound can be eliminated, making the process independent on different slowly varying

influencing factors. This means that a spirometer using this principle does not need to be calibrated.

1.3.3 Wireless Spirometers



(a) Spirobank II Smart [25]



(b) SpiroSonic MOBILE [26]



(c) EasyOne[®] Air Spirometer[27]

Figure 1.11: Different wireless spirometers

1.3.3.1 Spirobank II Smart

The Spirobank II Smart Spirometer is manufactured by MIR Inc. ,USA. It has a liquid crystal display (LCD) and can therefore be used stand-alone or in conjunction with an iPad or a personal computer (PC). The wireless connection with the iPad is made via Bluetooth[®] Classic, while the connection with the PC is only possible via universal serial bus (USB). Software for carrying out and evaluating the examination are available for both, tablet and

PC (included in the purchase). It is powered either via USB or by a Lithium-ion battery pack with a voltage of 3.7V and charge of 1100mAh (which is also charged via USB). With the power supply via the battery pack, 40h operating hours are guaranteed by the manufacturer. The respiratory flow is measured using a turbine. Although it is described in literature that spirometers with this measurement method must be calibrated regularly[7], this is not necessary according to the manufacturer.[25]

1.3.3.2 EasyOne® Air Spirometer

The EasyOne® Air Spirometer is manufactured by ndd Medizintechnik AG, Switzerland. It has a touchscreen and can be used stand-alone or in conjunction with a PC. The wireless connection with the PC is established via Bluetooth® Classic. The manufacturer provides software that can be used to perform tests and generate reports with the results. The spirometer comes with a charger and, according to the manufacturer, can perform up to 100 worth of tests on a single charge. The respiratory flow is measured using ultrasound. More specifically, the company's proprietary TrueFlow™ method is used. These devices do not actually need to be calibrated[7][28], as the measurement is made using two opposing ultrasonic waves, which cancels out the ambient conditions. [27]

1.3.3.3 SpiroSonic MOBILE

The SpiroSonic MOBILE Spirometer is manufactured by Uscom Kft., Hungary. It must be connected to a PC via USB or Bluetooth® Classic or to an Android device via Bluetooth® Classic. The manufacturer provides software for PC and Android devices. It is powered via USB or via a 3.7V battery. No operating time is specified. The respiratory flow is also measured here using ultrasound, which means that regular calibration of the device is not necessary.[26]

1.4 Aim of this thesis

The aim of this master thesis is to build an air flow sensor based on differential pressure measurement. The relationship between differential pressure and air flow is to be determined based on the simplest possible correlation.

The measured differential pressure is to be transmitted to a receiving device via Bluetooth[®] Low Energy. A script in MATLAB[®] or Python[™] is to be developed to calculate the respiratory flow and respiratory volume from this data and to display them graphically.

Materials and Methods

2.1 Concept

To be more flexible in the development process, the wireless spirometer concept was divided in two parts. The first part is the tube through which the breathing air flows. The second part is a PCB on which the sensor or sensors and subsequently the MCU are soldered. The concept is illustrated in Figure 2.1. By splitting them up, all parts can be developed or further developed independently of each other, which allows a more flexible development process.

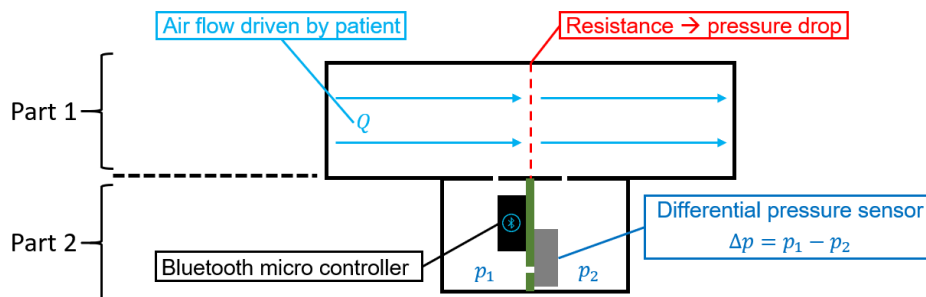


Figure 2.1: Drawing of wireless air flow sensor concept

2.2 Hardware

This section describes the realisation of the hardware of the wireless airflow sensor. This includes electronic components as well as 3D printed mechanical components.

2.2.1 Electronic Components

When selecting the main electronic components, such as the MCU and also the digital differential pressure sensor, the Infineon Technologies AG product portfolio is primarily used. The main focus is on energy consumption, the fulfilment of the measurement requirements with regard to the quantity to be measured and, in the case of the MCU, the version of the Bluetooth[®] specification.

2.2.1.1 Microcontroller Unit

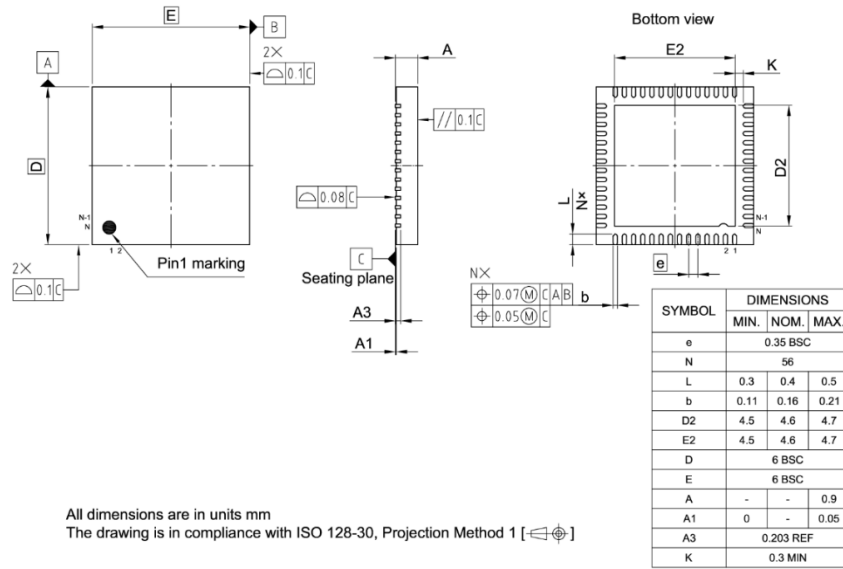


Figure 2.2: Drawing of the QFN-56 package in with the AIROC[™] CYW20829 comes. [29]

The Infineon PSoC™ and AIROC™ portfolios have a wide range of MCUs that enable wireless communication, good integrability and low power consumption. The AIROC™ CYW20829 ultra-low-power Bluetooth® LE 5.4 was chosen, because it is the latest one with Bluetooth® LE 5.4 specifications. It has two ARM Cortex M33 processors. While the first processor is clocked with 96 MHz and is executing the application, the second one is clocked with 48 MHz and is only managing the Bluetooth® sub system. The transmission power of the Bluetooth® sub system can be configured up to 10 dBm. It also has a robust receive sensitivity of -106 dBm. The required IIC or SPI interfaces are provided as well. It also has many other interfaces (see Figure 2.3), but these are not used for the realization of this work. The MCU is packaged in a 56-lead QFN (quad flat no-lead) 6.0 x 6.0 x 0.9 mm package, as displayed in Figure 2.2.

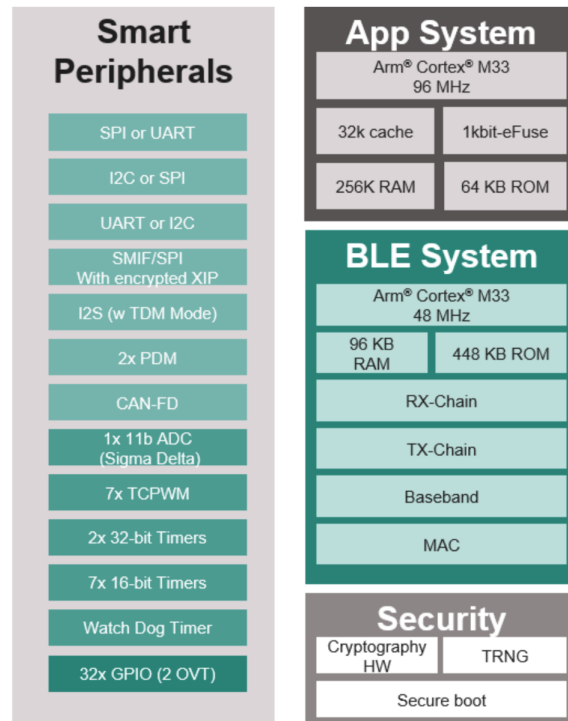


Figure 2.3: Block diagram of the CYW20829 with its peripherals and sub systems. [30]

2.2.1.2 Digital differential pressure sensor

The DDPS is the differential pressure sensor of choice. The main advantages of the sensor are its low power consumption, good accuracy and outstanding precision. The sensor is connected to the MCU via IIC, as shown in Figure 2.4, in order to be able to use the interrupt function. Due to the requirements discussed in chapter 1.2.2.2 regarding the sampling frequency, this is set to $f_s = 128\text{Hz}$. The oversampling rate is set to $OSR = 2$ (see table 1.2). In addition, the configuration of the sensor has been designed to prompt an interrupt whenever a new pressure value is ready. This feature critically conserves the energy that the MCU would otherwise have to expend in the process of repeatedly polling the sensor for data.

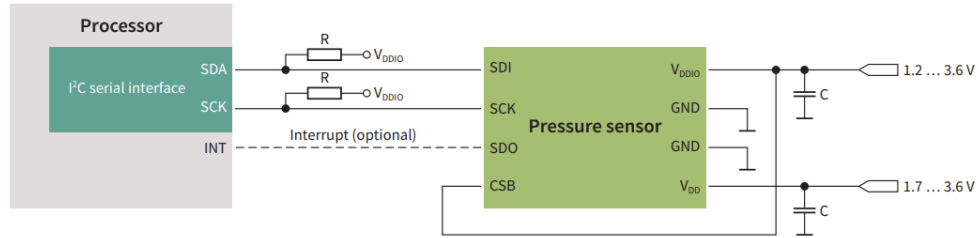


Figure 2.4: DDPS connected to the MCU via IIC with two pull up resistors and optional interrupt connection.

2.2.2 Circuit Design

The Altium Designer® Version 22.2.1 programme from Altium Europe GmbH was used to develop the electronic circuits within this thesis. This is a widely used programme for the development of individual Printed Circuit Boards (PCBs) through to entire devices. There are standard libraries with the most frequently used components, but one can also create one's own symbols and footprints. The PCB design process was carried out as follows:

- Compilation of all required components in a component library. Infineon already has a huge library of standard components and its own products. However, as the differential pressure sensor and MCU used are not present in this library, the symbols and footprints had to be created using Altium Designer®.

- Create the schematic circuit diagram. The symbols of the components used are inserted and electrically connected in this step.
- Creating the printed circuit board. In this step, the shape of the PCB and the dimensions of the individual layers are defined. For the latter, the manufacturer's offers must be used as a guide.
- Placing the components on the PCB.
- Routes of the electrical connections between the components.
- Creation of the production data.

2.2.3 Circuit Manufacturing

The designed PCBs were manufactured by Multi Leiterplatten GmbH. During the design process, care was taken to adhere to the design guidelines for standard production in order to be able to produce as cost-effectively as possible. This includes PCBs with up to 8 layers, FR-4 as the carrier material between the layers. This is a heat-resistant composite material made of epoxy resin and glass fibre fabric. The minimum track width is 100 μm , the minimum hole diameter is 200 μm . The contact points for components have a finish made of Electroless Nickel Immersion Gold (ENIG), which is intended to prevent corrosion during prolonged storage.

2.2.4 3D Design

In the course of this work, mechanical components were also developed using Inventor® Professionel - 2023 from Autodesk GmbH. This offers mechanical design, documentation and product simulation. The 3D design process was carried out as follows:

- Creating several individual simple components
- Joining the individual components to form an assembly
- Export of the assembly in STL format so that it can be produced in the 3D printer

All drawings created are attached in the appendix under B.

2.2.5 3D Printing

For printing the 3D designed parts within this work, the Bambu Lab X1-Carbon manufactured by Bambulab GmbH was used. The material used for printing was black colored polylactic acid.

2.3 Spirometer V1

The design of the Spirometer V1 has been developed primarily for the characterisation of the membrane. The system consists of two parts:

- **A:** flow element V1
- **B:** sensor PCB V1

Part **A** and **B** are connected to each other via pneumatic connections and a pneumatic hose, as displayed in Figure 2.5. This design makes it possible to replace the parts quickly if necessary. The connections and the hoses in turn guarantee absolute air tightness of the system.

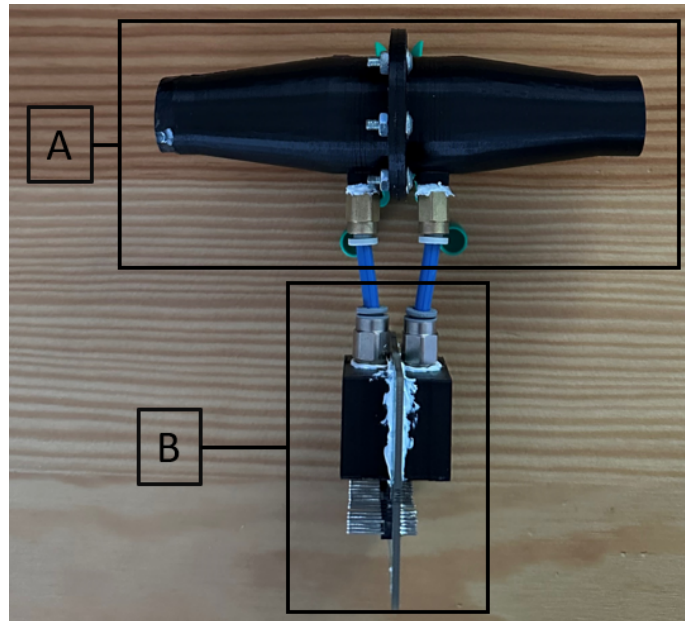
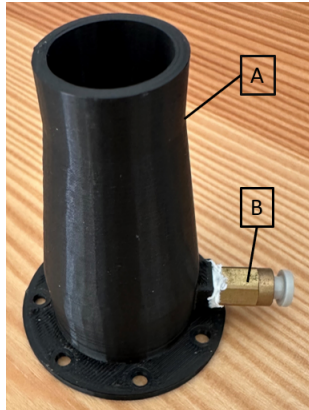
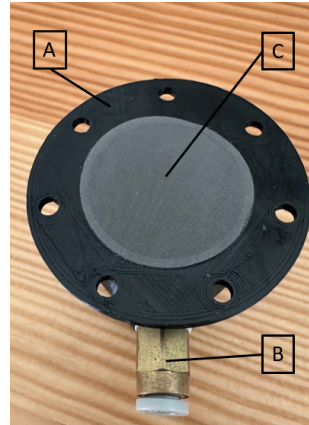


Figure 2.5: Spirometer V1 system. Part A is the flow element V1. Part B is the sensor PCB V1.

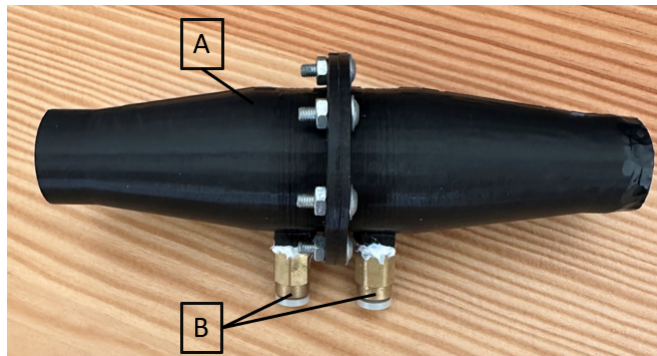
2.3.1 Flow element V1



(a) Side view of one flow element half with screwed and glued pneumatic connector.



(b) Inside of the flow element with placed Lilly membrane.



(c) Assembled flow element V1

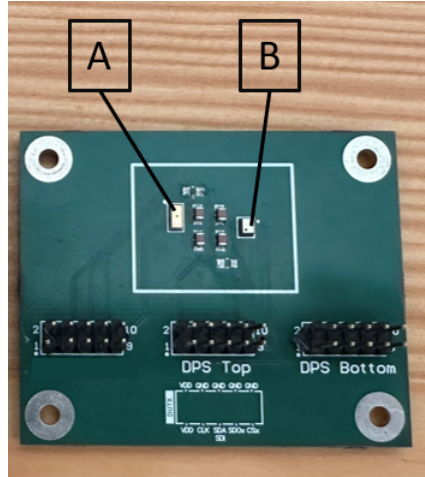
Figure 2.6: 3D printed parts of the flow element V1. Part A is the pipe through which the air flows. Part B is the screwed and glued pneumatic connector. Part C is the Lilly membrane (flow resistance).

The flow element V1 was designed so that its flow connections fit on the ndd Easy on-PC spirometer described in chapter 2.5.1. The design drawing can be viewed in the appendix (B.1). The two identical halves were 3D printed separately. The membrane was placed between the two halves and these were then screwed together. To connect the flow element to the sensor module, an

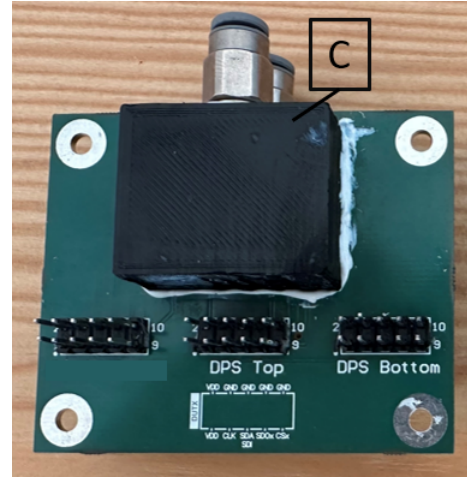
M4 thread was cut into the existing hole located before and after the membrane and a pneumatic connection was inserted. Silicone adhesive was also used to guarantee tightness. The finished assembled flow element is shown in Figure 2.6c.

2.3.2 Sensor PCB V1

The sensor PCB V1 is a simple two layered design. It holds the DDPS and a decoupling capacitance for the supply of the sensor. Furthermore, two DPS368 (described in 1.2.5), one on top, one on bottom, were also attached with a capacitance each. In the early stages of this work, it was considered to use two DPS368 instead of the DDPS, if the sensor does not work as expected. Since this PCB was the first test of the designed footprint, it was not certain whether the communication with the sensor would work and whether the ventilation of the bottom pressure inlet was given. A 3D printed chamber is glued onto the PCB to seal the sensor airtight from the environment. The design drawing can be viewed in the appendix (B.3). Pneumatic connections were also screwed into the chamber to connect it to the flow element. The pins of the sensors can be accessed via the pin headers.



(a) PCB without chamber.



(b) PCB with glued chamber

Figure 2.7: Sensor PCB. Part A is the DDPS. Part B is the DPS368. Part C is the 3D printed chamber.

2.4 Spirometer V2

The Spirometer V2, hereinafter always referred to as IFX-Spirometer, consists of three parts.

- **A:** flow element V2
- **B:** sensor PCB V2
- **C:** bacteria filter

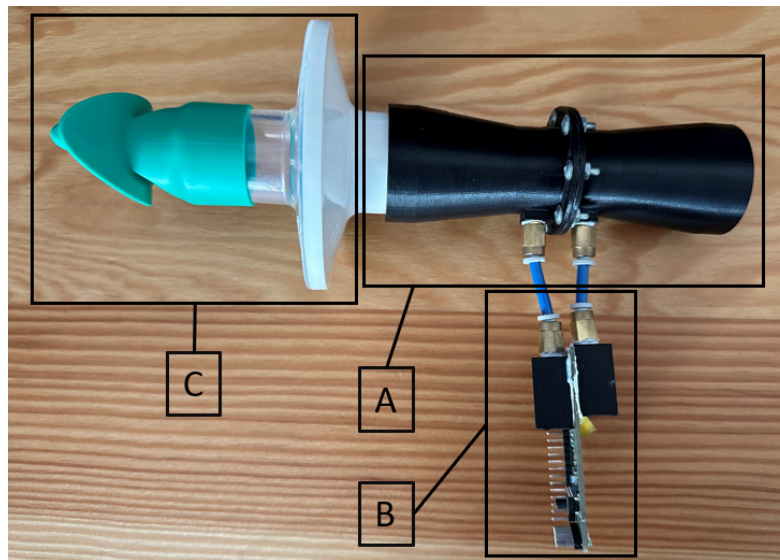


Figure 2.8: SpirometerV2. Part A is the flow element, Part B the sensor PCB, Part C the bacteria filter for spirometry.

2.4.1 Flow element V2

The design of the flow element V2 has been modified so that a bacterial filter developed for spirometry can be fitted in front of the flow element. This is necessary for hygienic reasons alone and also laminarises the turbulent exhaled air due to its filtering membrane. A detailed drawing can be found in the appendix under B.2.

2.4.2 Sensor PCB V2

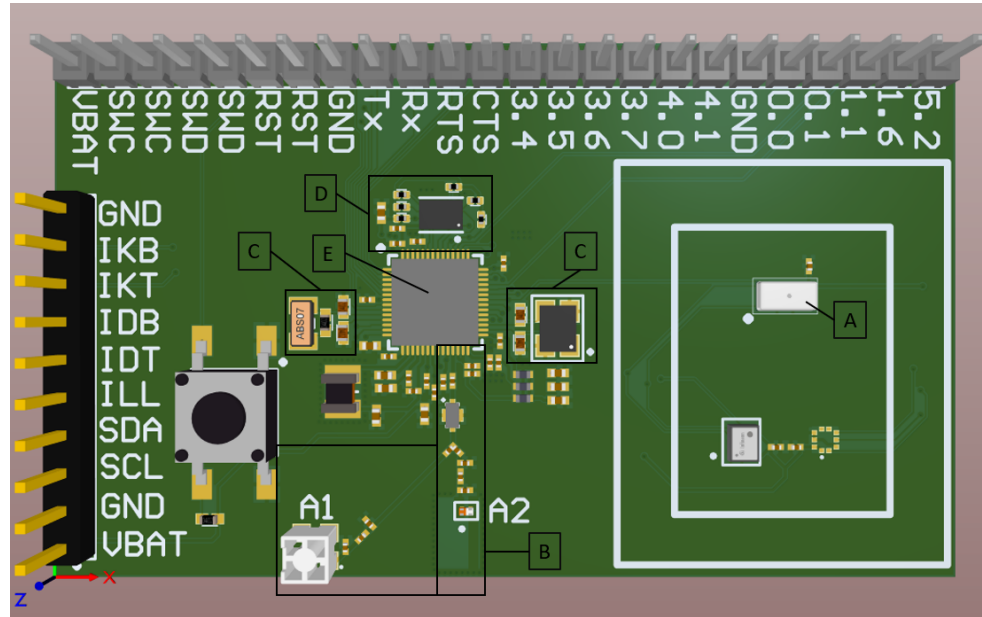


Figure 2.9: Design of the Sensor PCB V2. Part A is the DDPS. Part B is the antenna path. Parts C are the two external crystal oscillators. Part D is the external QSPI flash. Part E is the AIROC™ CYW20829.

The sensor PCB V2 should enable a first proof of concept for the entire wireless BLE spirometer system. The PCB is 50 x 30 mm in size and is a four layer PCB. All components are placed on layer 1 (top layer). Furthermore, all critical traces such as the antenna path, traces to the oscillators, power supply traces of the voltage regulators and, where space permits, some non-critical traces such as GPIO and IIC traces are also present on this layer. The designed PCB consists of two areas. Only the DDPS (Part A in Figure 2.9) is positioned in the first area. A white double frame is drawn around the DDPS, which marks exactly the area on which the pressure chamber needs to be glued. The MCU (Part E in Figure 2.9) with all required peripheral components and a button (Part G in Figure 2.9) for resetting the MCU is placed in the second area. This includes a 24 MHz crystal oscillator and a second crystal oscillator with 32.768 kHz. In addition, the AIROC™ CYW20829 requires an external QSPI flash (Part D in Figure 2.9). This serves as an exten-

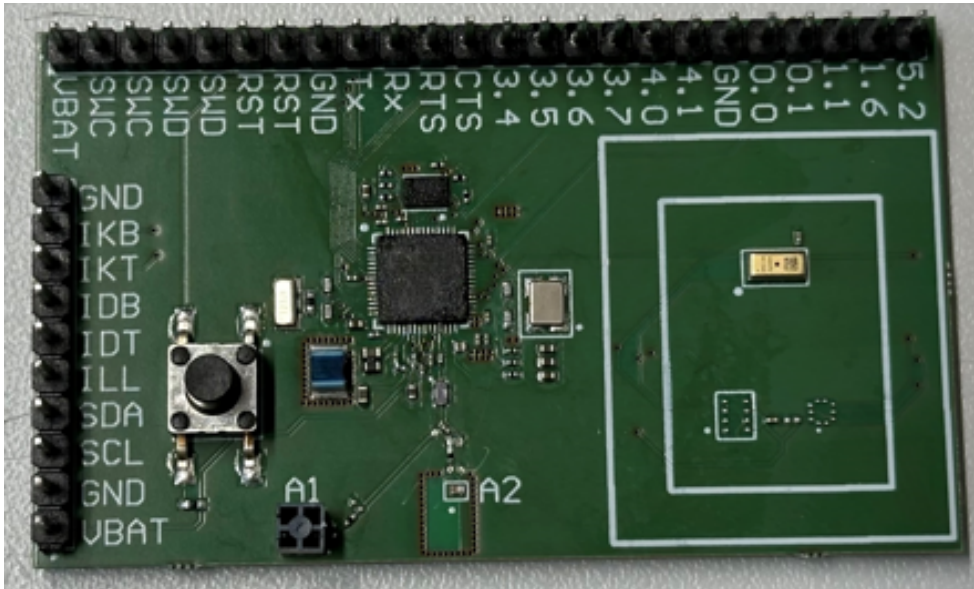


Figure 2.10: Picture of the populated sensor PCB V2

sion to the internal memory and is required to store the firmware. To make debugging easier, all GPIO pins of the MCU are routed to a pin header. This makes it possible to receive debugging messages from the MCU via UART. Furthermore, it is easy to react to potential design errors regarding the pin assignment.

2.5 Characterization of Lilly mesh

To convert the laminar breathing air flow into a differential pressure, a fine-meshed membrane according to **Lilly** (as described in section 1.3.2.1) is used. The relationship is linear in laminar flow and is therefore the greatest advantage of this principle. The membrane used was provided free of charge by the Technical University, Institute for Biomedical Imaging. It was manufactured by Schiller Handelsgesellschaft m.b.H, based in Linz, Austria. As the company did not respond to request regarding the characteristic of the membrane, the relationship between differential pressure and respiratory air flow had to be determined experimentally.

2.5.1 Measurement setup

A wind tunnel, which is driven by a DC fan, provides the laminar air flow. The fan has a rated voltage of $V_N = 12\text{V}$ and a maximum current consumption of $I_{max} = 4\text{A}$. The fan is driven and controlled by an adjustable voltage source. The turbulent air is laminarised by means of a net directly after the fan and a honeycomb structure. The duct is then narrowed so that the flow sensor can be connected. The ndd Easy on-PC spirometer from ndd Medizintechnik AG is used as the flow sensor. The signal corresponding to the air flow is transmitted to the PC via USB. Afore mentioned company also provided a scientific software called WBreath, which enables to access all raw data from the Easy on-PC spirometer. This made it possible to use it as a flow sensor. The Lilly spirometer with the membrane is connected directly after the flow sensor. A picture of the measurement setup is illustrated in Figure 2.11. The differential pressure is measured by the DDPS and transmitted to the PC via a NI-USB-8452 manufactured by National Instruments, which is an USB-IIC/SPI interface.

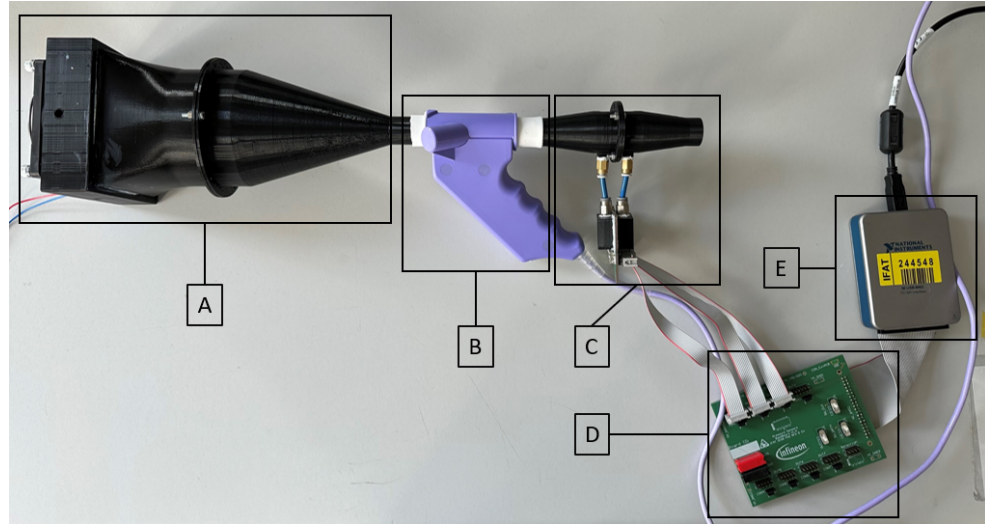


Figure 2.11: Image of the measurement setup. Part A is the wind tunnel. Part B the Easy on-PC spirometer. Part C ist the spirometer system V1. Part D is a interface PCB. Part E is a NI USB-8452 IIC/SPI interface.

The maximum laminar flow that can be generated by the previously de-

scribed fan is $Q_{max} = 4 \frac{1}{s}$. The minimum laminar flow is $Q_{min} = 0.71 \frac{1}{s}$. This is the flow point which is reached at the minimum supply voltage of the fan. To obtain as much data as possible, the step size in this range is set as finely as possible. Starting from $Q_0 = Q_{min}$, the second measuring point is at $Q_1 = 1 \frac{1}{s}$. Then Q is increased equidistantly in $0.25 \frac{1}{s}$ steps up to $Q_{max} = 4 \frac{1}{s}$. For each flow, the DDPS samples $N = 100$ differential pressure samples. In this way, noise can be reduced by averaging.

2.5.2 Fitting

The relationship between differential pressure Δp and volume flow Q , the so called flow resistance R (see Equation 1.3) is already known from the chapter 1.2.3. To calculate the flow resistance R from the measured data set, a linear regression is used, which is forced through the origin. A model without an offset was chosen because the offset from the bridge and the ADC of the sensor is already compensated as part of the temperature compensation. The following model is used for this purpose [31]:

$$y_i = \beta_1 \cdot x_i + \epsilon_i \quad (2.1)$$

With y_i as dependent variable, x_i as independent variable, β_1 as parameter, which is to be estimated and ϵ_i as error. The following equation is now introduced to determine the parameter β_1 with the method of least squares:

$$\beta_1 = \frac{\sum x_i \cdot y_i}{\sum \Delta x_i^2} \quad (2.2)$$

If the variables of equation 1.3 are inserted into equation 2.1 and 2.2, the result is obtained:

$$\Delta p_i = R \cdot Q_i + \epsilon_i \quad (2.3)$$

$$R = \frac{\sum \Delta p_i \cdot Q_i}{\sum Q_i^2} \quad (2.4)$$

The fitting model is implemented in MATLAB® [32] as follows:

```
oFittype = fittype('a*x','independent','x','  
dependent','y','coefficients','a');  
oFitOfResistance = fit(vQ,vDP,oFittype);
```

With the function "fittype" the model is defined. The vectors vQ and vDP are holding the data, where vDP is the mean value of the 100 measured differential pressures.

2.6 Firmware

This section describes the selection of the used integrated development environment (IDE) and the development of the firmware that is running on the MCU.

2.6.1 IDE and evaluation kit

Infineon Technologies AG provides the ModusToolbox™ to develop firmware for the selected AIROC™ CYW20829. This is a collection of development tools, middleware, device drivers and code examples. ModusToolbox™ supports several IDEs like Arm μ Vision, IAR Embedded Workbench, Microsoft Visual Studio Code and Eclipse IDE. Infineon Technologies recommends the use of Eclipse IDE for ModusToolbox™ [33]. The version used in this work is ModusToolbox™ 3.1. Two of the many provided tools within ModusToolbox™ are the device configurator 4.10 and the Bluetooth® configurator 2.80. Within the device configurator, the behavior of the serial interfaces, the ADC, the timers and the GPIOs can be configured using a graphical user interface (GUI). Within the Bluetooth® configurator, the GAP and GATT properties of the BLE device can be configured using a GUI. The custom service and characteristics used within the firmware were created with this tool. For testing the developed firmware, the AIROC™ CYW20829 Bluetooth® LE SoC evaluation kit in combination with a PCB, which has a sensor on it, was used. The PCB holding the sensor is called Sensor PCB V1. The supply, interrupt pin, ground and IIC pins of the two boards were connected, as illustrated in Figure 2.12.

2.6.2 Custom service and characteristic

A custom service is first created in the Bluetooth® Configurator 2.5 which groups all relevant properties of the DDPS. It serves as a container for the following characteristics, which then contain the actual data to be transmitted. The service is called IFX Pressure Sensor. The Bluetooth® Configurator 2.5 generates a random UUID (which is not registered in the list of SIG) when creating the service.

The process is quite similar for creating a custom characteristic. The first

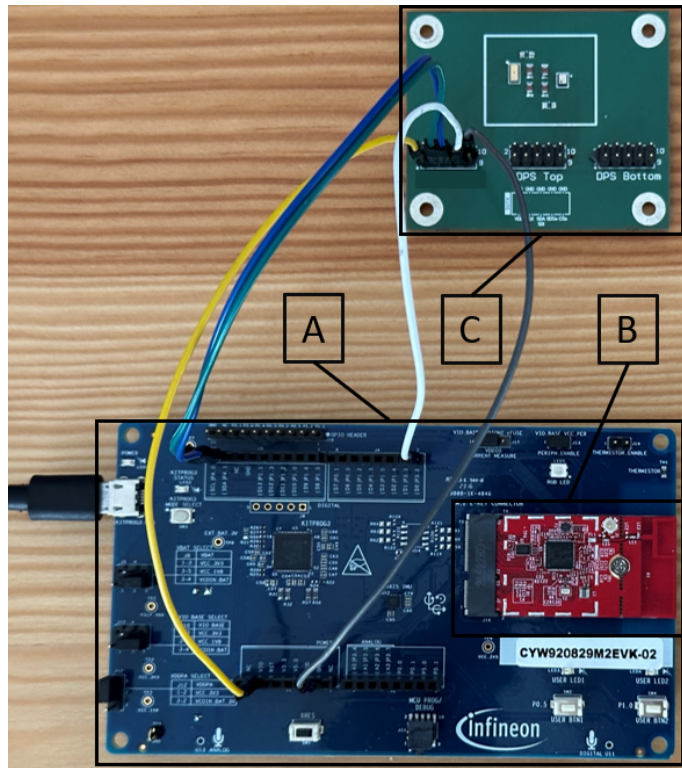


Figure 2.12: AIROC™ CYW20829 Bluetooth® LE SoC evaluation kit (Part B) connected with the sensor PCB V1 (Part C). Part B is the module with the micro controller and all required peripheral components and also the antenna.

characteristic is called Pressure and Temperature and is illustrated in Figure 2.13. This custom characteristic got assigned a randomly generated UUID as well. The data type, length and initial values for the characteristics can be defined in the "Fields" line highlighted in grey. The selected DDPS provides the differential pressure and temperature data with 24bit each. A uint8 array with a length of six fields is therefore sufficient. In the properties, "Read" and "Notify" are selected to allow the central device to read the characteristic and to enable the server to send notifications to the central device as soon as new data is available. Additionally, separate characteristics were created for the calibration coefficients and sensor id. For this two characteristics only the "Read" property is selected since this sensor specific information is transmit-

ted only once as soon as the connection is established.

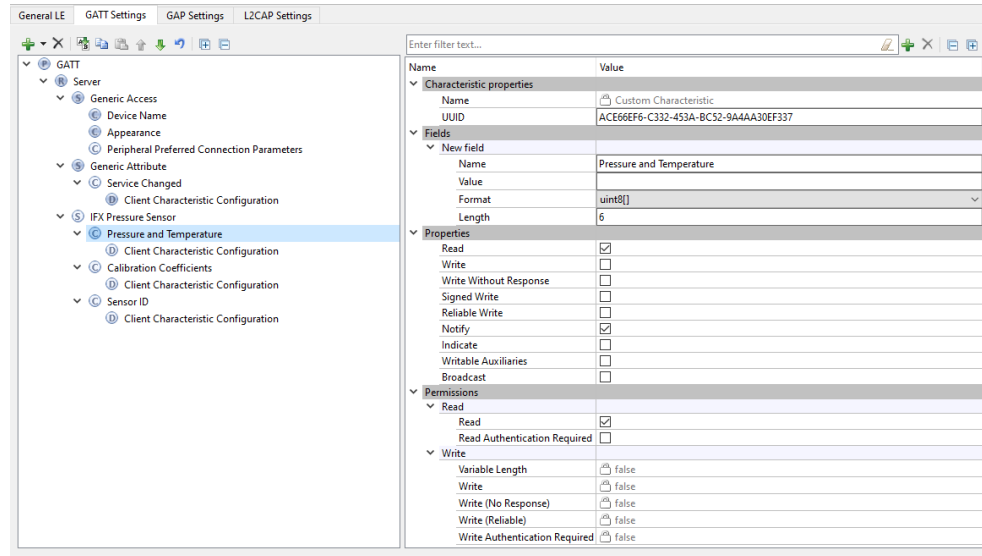


Figure 2.13: Bluetooth® Configurator 2.5 with the GATT database visible on the left column with the selected custom characteristic Pressure and Temperature. The right column shows the properties of the custom characteristic.

2.6.3 Program Flow

The development of the firmware is based on RTOS. Infineon Technologies AG is a developing partner of FreeRTOS™, which is distributed freely under the MIT open source license[34]. FreeRTOS™ is included with ModusToolbox™ 3.1 for the AIROC™ CYW20829.

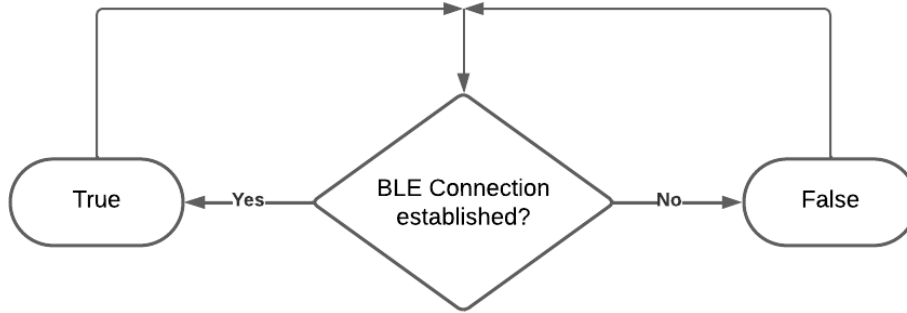


Figure 2.14: Event 1 - query of the state of the connection

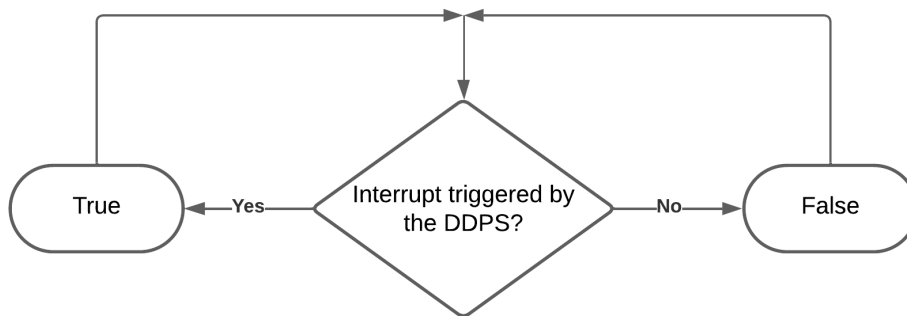


Figure 2.15: Event 2 - query of the state of the interrupt.

As discussed in chapter 1.2.6, a RTOS program is made up of tasks. These are queued by the task sheduler based on their priorities. The developed firmware consists of two tasks, which are executed based on an associated event. The first task is referred to below as the Connection task. Its purpose is to establish a BLE connection with a central device. It is triggered by Event 1, shown in Figure 2.14. The second task is referred to below as the Notify task. Its purpose is to read the differential pressure and temperature data from the sensor, write it to the GATT-database and then send a notification to the central device. It is triggered by Event 2, shown in Figure 2.15. The main program flow is illustrated in Figure 2.16 and proceeds as follows.

As soon as the system is supplied, it starts with the initialization. During the initialization the later used blocks like the Bluetooth® stack, the GATT database, the IIC interface and the ISR for triggering Event 2 are enabled first. Next, the DDPS is configured via IIC. The calibration coefficients and the sensor id are also read from the DDPS via IIC and written to the GATT database. The DDPS then remains in a low power state, as no sensor data is yet required and energy can therefore be saved. Next, the task scheduler is started and the Connection task is executed, until a BLE connection with a central device is established. If the connection process is successful, the DDPS is set to continuous sampling mode via IIC. The DDPS is now triggering the ISR, as soon as new data is available. The ISR sets a flag which in turn triggers the Notify task. The latest differential pressure and temperature data are read from the DDPS via IIC and are written to the GATT database. If the central device has notifications enabled, a notification with the new data is sent to the central device. If the connection to the central is lost, the sampling of data is stopped via IIC and the connection process starts all over again. The flag, which is previously set by the ISR, is cleared at the end of the Notify task.

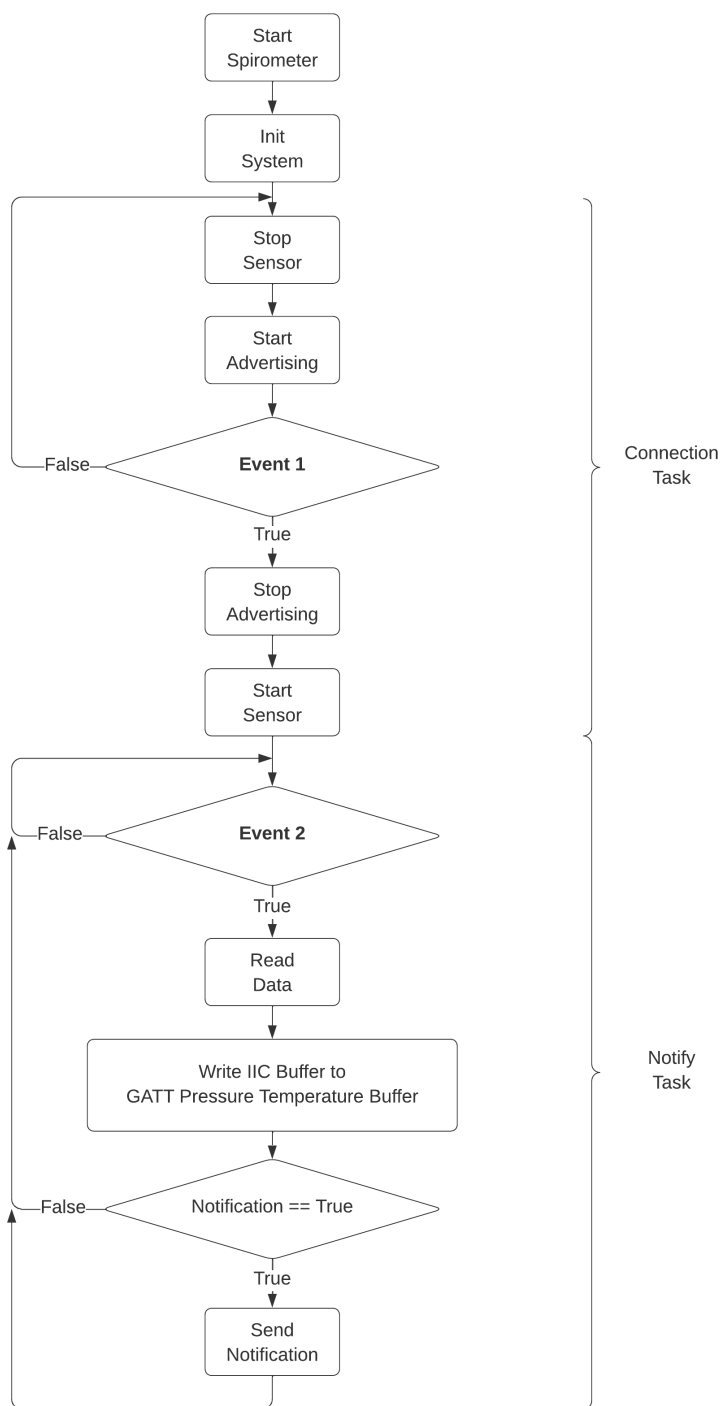


Figure 2.16: Main program flow of the developed firmware running on the AIROC™ CYW20829

2.7 Software

In this section the software for handling BLE communication, data processing as well as data visualization, is explained.

2.7.1 BLE server

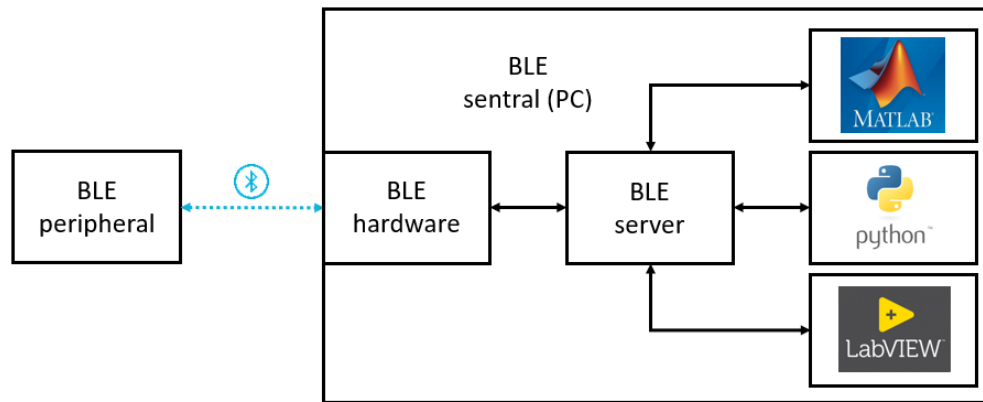


Figure 2.17: Sketch of the signal chain using the BLE server

Infinion has developed its own interface to interact with BLE peripherals or receive high throughput data from peripherals. It is a .NET-application and developed in C#. This interface is subsequently referred to as the BLE server. The BLE server has direct access to the BLE hardware of the PC and can therefore read and buffer the received data. The server also opens a so-called publisher, which can be used to retrieve the data. This publisher can then be accessed using any tool such as MATLAB®, Python™ or LabVIEW™. Since the tools mentioned above have inadequate and usually very slow interfaces to BLE, this BLE-server offers a good solution to achieve a stable BLE communication between the central and the peripheral device. To receive the data from the spirometer, only the UUID, data type and data length of the corresponding characteristics and the UUID of the service must be communicated to the BLE server.

2.7.2 MATLAB® Script

MATLAB® was selected as the tool for connecting to the BLE server. A script was created that connects to the BLE server, receives, processes and visualises data.

2.7.2.1 Connection with the Spirometer V2

To establish a BLE connection with the Spirometer V2, the BLE server library has to be loaded within the script. Now the connection between MATLAB® and the BLE server can be established. If the connection to the server was successful, the discovery process can be started and connection can be established to the desired device. After establishing a connection, the BLE server reads the Calibration Coefficients characteristic from the GATT database and enables the notification of the Pressure and Temperature characteristic. Now the connected Spirometer V2 module is streaming the differential pressure and temperature data continuously to the BLE server. To transfer the data from the BLE server to the MATLAB® script, the length of the signal to be sampled must be provided. The script is calculating the number of samples based on the desired signal length and the sampling frequency to calculate the number of samples. The data is transferred until the target number of samples has been reached.

2.7.2.2 Post processing

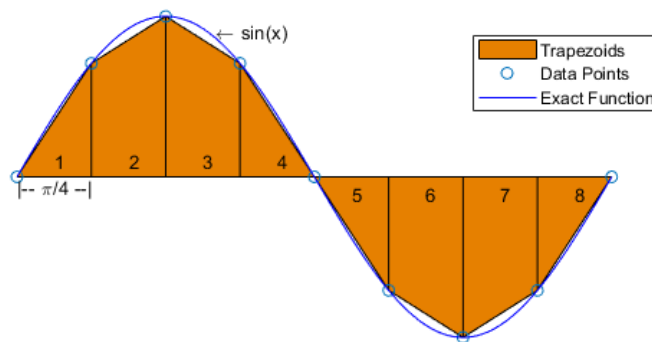


Figure 2.18: Example of the numerical integration of a sinus using trapezoidal method[35].

The data received is 24-bit for both the differential pressure and the temperature. With the calibration coefficients received, a temperature-compensated differential pressure value Δp can now be calculated with the implementation of the equation 1.7. Next, the identified model of the flow resistance R of the Lilly membrane is used to calculate the flow. The flow needs to be integrated over time to get the volume. Since the recorded data is a discrete-time function, the integration must be carried out numerically. The numerical trapezoidal integration method, which is shown in Figure 2.18, is already implemented in MATLAB®. The approximation of the integral from equation 1.1 is calculated as follows:

$$V = \int_{t_1}^{t_N} Q(t) \cdot dt \approx \frac{t_N - t_1}{2 \cdot N} \sum_{n=1}^N (Q[t_n] + Q[t_{n+1}]) \quad (2.5)$$

The trapezoidal rule is often sufficient for integrating flow signals in spirometry due to its simplicity and robustness against noise. In contrast, Simpson's rule, which relies on quadratic interpolation, can be more sensitive to noise, potentially leading to larger errors when applied to noisy data. This increased sensitivity arises because the higher-order polynomial approximations used in Simpson's rule can amplify the effects of noise present in the data. [36]

2.7.2.3 Calibration and BTPS correction

The implementation of the calibration process was also realized within the MATLAB® script. Therefore a 2l calibration syringe provided by the TUG was used. The total 2l is dispensed several times in succession. The results of the measured volume are averaged and a correction factor is applied in accordance with:

$$c_s = \frac{V_{pump}}{V_{measured}} \quad (2.6)$$

The correction factor c_s is used to correct the actual measured flow. As the factor is not time-dependent, it can be included in the integral of equation 1.1 and can therefore be applied directly to $Q(t)$. This calibration routine has to be performed on a regularly basis when using the device, for example every morning or even twice a day. However, as Infineon Technologies AG does not have a calibration pump at the time of writing, this step can also be skipped. The factor $c_s = 1$ is used in that case.

The correction of the BTPS conditions is implemented for the inhaled and the exhaled air. As there is a lack of the necessary measuring equipment to establish the BTPS conditions, the value from [10] is used. There it is described that 1 l volume of ambient air corresponds to approximately 1.1 l lung volume. If a positive flow (inhalation) is detected, this is multiplied by the factor $BTPS_{in} = 1.1$. For the same reason and since the temperature difference between the air in the lungs and the air at the sensor is only minimal, the factor $BTPS_{ex} = 1$ is used.

The following condition is therefore implemented for computing the corrected flow $Q_{cor}(t)$ out of the measured flow $Q_m(t)$:

$$Q_{cor}(t) = \begin{cases} c_s \cdot BTPS_{in} \cdot Q_m(t) & \text{if } Q_m(t) \leq 0 \\ c_s \cdot BTPS_{ex} \cdot Q_m(t) & \text{if } Q_m(t) > 0 \end{cases} \quad (2.7)$$

2.8 Module performance

In this section, the Spirometer V2 developed is compared with a state of the art spirometer. Furthermore, the power consumption is analysed to get an impression of the energy consumption of the developed module.

2.8.1 Comparison to the ndd Easy on-PC spirometer

For a comparison between the build spirometer V2 module (consequently referred to as IFX-Spirometer) and a state of the art Easy on-PC spirometer (consequently referred to as US-Spirometer), a measurement with both spirometers connected was performed. To generate the test data, the maximum exhalation and the maximum inhalation of a 29 year old male subject were measured. The WBreath software from ndd was used to record the signal using the US-Spirometer. The data recorded with the US-Spirometer was sampled with 100Hz. The developed MATLAB[®] script was used to sample the data from the IFX-Spirometer. The BTPS correction factors of the US-Spirometer were used for the BTPS correction of both spirometers (see Figure 2.19). To compare the two spirometers, datapoints from both of the signals were taken and are compared within a correlation plot and a Bland-Altman plot. Since these plots need data sets of equal length, the data

from the IFX-Spirometer was sampled down from 128Hz to 100Hz using the MATLAB[®] method resample.

Inspiratory BTPS Correction

The inspiratory BTPS correction factor is computed using the values of ambient temperature, pressure and humidity. Ambient temperature and pressure are measured using two sensors. Ambient humidity, however, is user defined during the calibration.

$$\frac{T_{Body}}{T_{Amb}} \cdot \frac{P_{Amb} - P_{H_2O}(T_{Amb}, H_{Amb})}{P_{Amb} - P_{H_2O}(T_{Body}, H_{Body})}$$

Ambient Temperature [degC]: 22.98

Ambient Pressure [hPa]: 1013

Ambient Humidity [%]: 50

Body Temperature [degC]: 37

Computed factor:

1.102

Expiratory BTPS factor

The expiratory BTPS factor is user defined during calibration. The factor takes into account the cooling of air from mouth to flow sensor.

User defined factor: 1.03

Figure 2.19: BTPS correction factors determined by the ndd Easy on-PC spirometer, read out with the WBreath software.

2.8.2 Charge consumption and estimated lifetime

A current waveform analyser was used to measure the charge consumption and the average current consumption. The current can be integrated directly into the charge on the measuring device. To obtain an average consumption, the IFX-Spirometer was connected to the BLE server. As a result, it transmits continuously data to the BLE server. 100 measurements were recorded over a period of 5 seconds each.

CHAPTER 3

Results

3.1 Lilly membrane characterisation

This chapter presents the results of the characterization of the Lilly membrane.

3.1.1 Measurement

The result of the measurement described in chapter 2.5.1 is shown in Figure 3.1. Figure 3.1 describes the relationship between the set flow Q , which is plotted on the x-axis, and the measured differential pressure Δp , which is plotted on the y-axis. For each flow Q , 100 values of Δp were recorded. The relationship between Q and Δp is not perfectly linear. In Figure 3.2, the measurement results were processed statistically. Figure 3.2a shows the standard deviation of the 100 recorded differential pressure values per Q . This also appears to increase with increasing Q , but only by a maximum of around 0.7 Pa. Figure 3.2b shows the recorded data as a boxplot. In order to be able to compare the individual boxes with each other, the median value of each data set was subtracted from the data. A trend can be recognized according to which the boxes become larger with increasing Q . The largest outlier is at -2.28 Pa. These results indicate a very good precision of the DDPS when measuring differential pressure caused by flowing air.

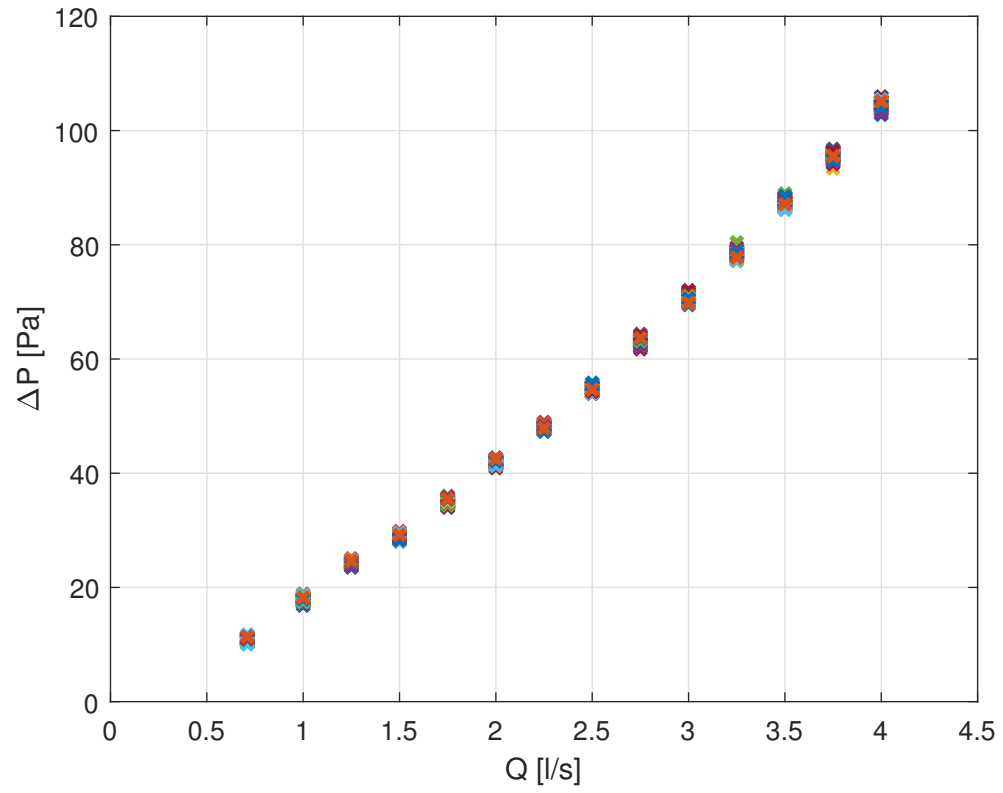
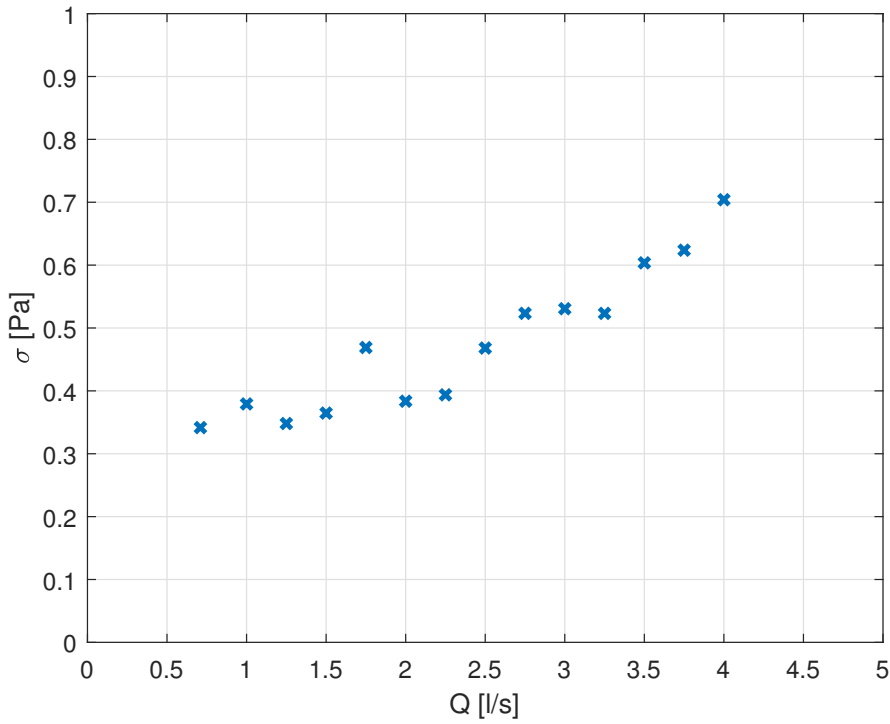


Figure 3.1: Relationship between applied flow Q and measured differential pressure Δp with 100 samples Δp per point Q .



(a) Standard deviation of the 100 differential pressure samples

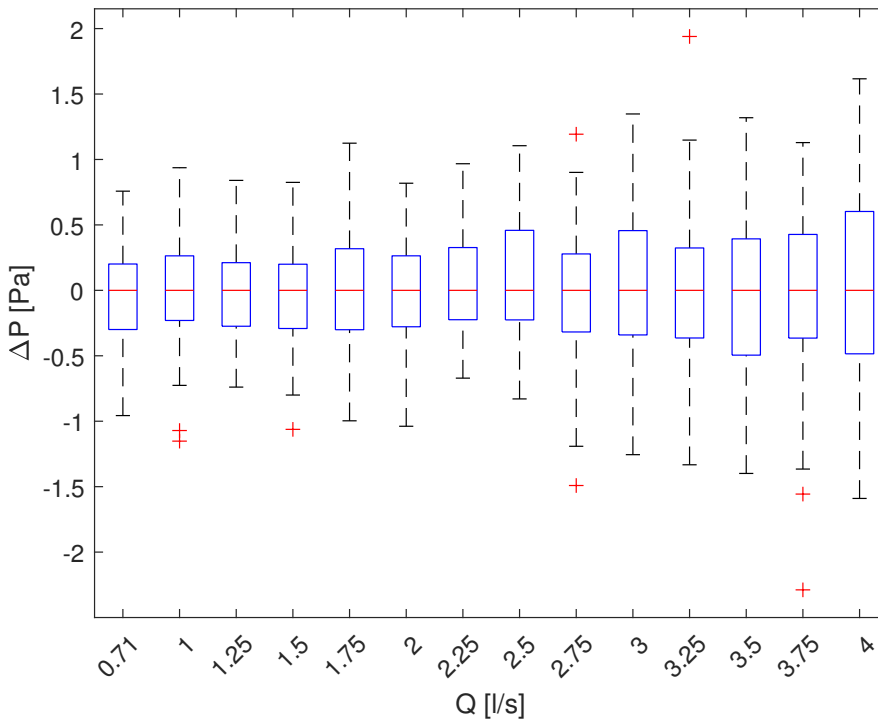
(b) Boxplot of the 100 differential pressure samples per flow point Q , minus the median value of each data set to be able to compare the data

Figure 3.2: Statistical evaluation of the measurement results from the characterization of the Lilly membrane

3.1.2 Fitting

The parameter determined using least square fitting is shown in Figure 3.3. A diagram of the relationship between differential pressure and flow is shown in Figure 3.4. The recorded differential pressure values are shown as blue dots. The red line represents the determined model. It seems to be, that the relationship between differential pressure and flow is not perfectly linear. However, the determined value $R = 23.76 \frac{\text{Pa}}{\text{l/s}}$ is subsequently used for the flow resistance. As already mentioned in Section 2.5.1, only a maximum flow of $Q_{max} = 4 \frac{\text{l}}{\text{s}}$ could be achieved.

```
val(x) = a*x
Coefficients (with 95% confidence bounds)
a =      23.76  (22.48, 25.04)
```

Figure 3.3: Identified model of the flow resistor

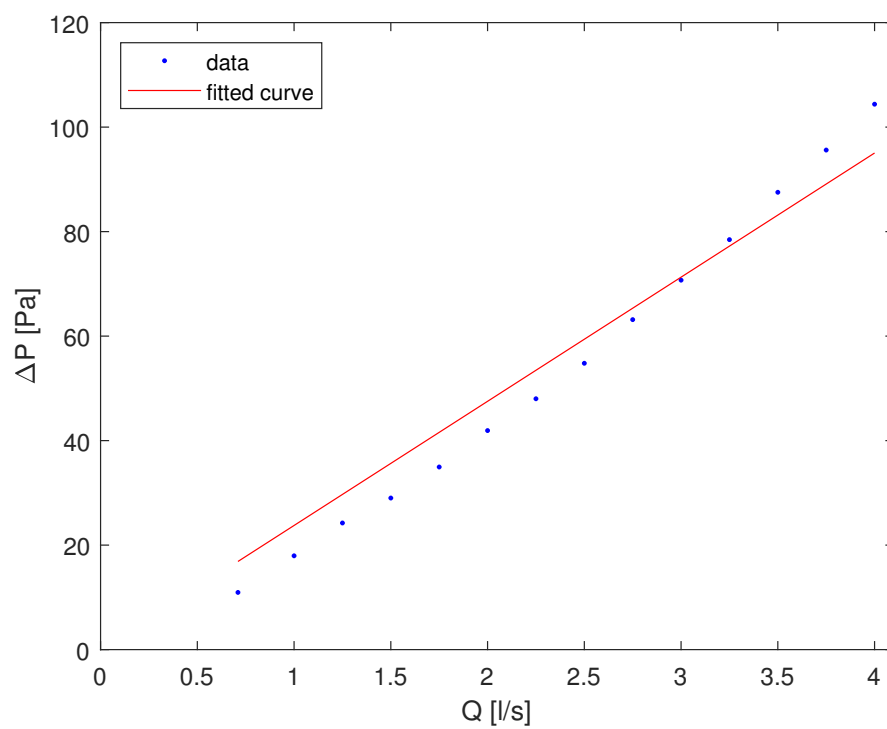


Figure 3.4: Data and fit which describes the relationship between Flow Q and differential pressure Δp

3.2 MATLAB[®] Script

This section shows the recorded measurement results which were measured with the IFX-Spirometer in combination with the BLE server and the developed MATLAB[®] script to verify a proper operating performance.

3.2.1 Differential pressure measurement

The following Figure 3.5 shows the differential pressure data measured with the IFX-Spirometer when a subject is breathing through the tube without the use of a filter. The negative part of the signal corresponds to the expiration, the positive part to the inspiration. It is noticeable that the negative half of the signal has significantly more noise than the positive half. This is due to turbulence that occurs in the airways during exhalation. Figure 3.6 shows the repetition of the measurement after attaching a filter to the flow element. Significantly less noise can now be observed during the exhalation phase. Thus, as assumed, the filter not only fulfils a hygienic function, but also ensures laminarisation of the exhaled air.

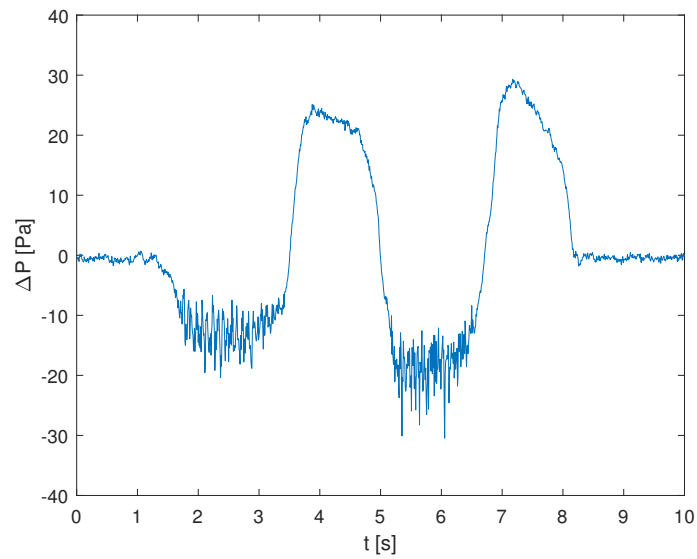


Figure 3.5: Differential pressure measured with the IFX-Spirometer without using a breathing filter

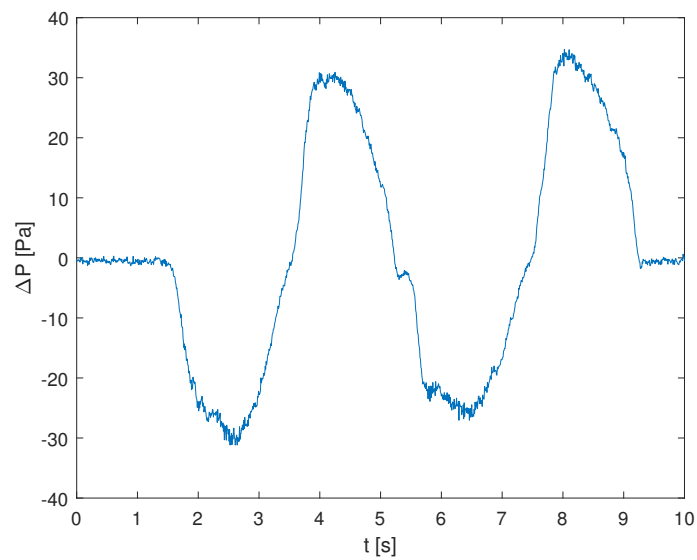


Figure 3.6: Differential pressure measured with the IFX-Spirometer using a breathing filter

3.2.2 Flow volume measurement

The following Figure 3.7 shows a flow and a volume curve, which was taken with the IFX-Spirometer and analysed by the MATLAB[®] script. The positive half-wave shows the inhalation flow, the negative half-wave the exhalation flow. The orange volume signal runs in a positive direction during the inhalation phase and in a negative direction during the exhalation phase.

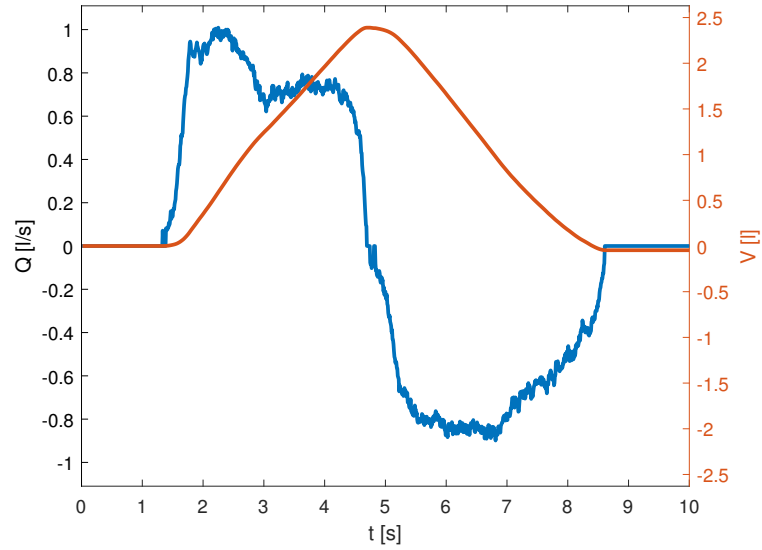


Figure 3.7: Flow and volume measured with the IFX-Spirometer. The blue curve is the air flow. The orange curve is the volume.

3.3 Performance of the IFX-Spirometer

This chapter presents the results of the calibration using a precisely defined volume, as well as the results of a comparative measurement with the Easy on-PC ultrasonic spirometer from ndd.

3.3.1 Calibration

The results of the three calibration runs can be seen in Table 3.1. The calibration factor c_s was calculated using the calculated mean value, which can also be seen in Table 3.1, and the defined volume of the calibration syringe.

The calculation is performed in equation 3.1. This calibration factor is used in the following section 3.3.2.

Calibration Run	Volume [l]
1	1.8974
2	1.9326
3	1.8736
Mean	1.9012

Table 3.1: Result of three calibration runs performed with a 2l syringe.

Using Equation 2.6, the calibration factor for this run results in:

$$c_s = \frac{V_{pump}}{V_{measured}} = \frac{2l}{1.9012l} = 1.052 \quad (3.1)$$

3.3.2 Comparison to Easy on PC

An inhalation and an exhalation phase with maximum lung volume were recorded. The exhalation phase is typically recorded as a negative flow. In the course of this measurement, the exhalation signal was also displayed as a positive flow in order to be able to better compare the following diagrams. To compare the two spirometers (IFX-Spirometer and US spirometer), the measured flow and the calculated volume of both devices were first plotted against time. In order to better recognise deviations, the recorded data from both devices were compared using a correlation diagram and a Bland Altman plot.

The measured flow signals of the exhalation (Figure 3.8) have the same waveform. Both signals exhibit a certain amount of noise, since each signal has an independent noise source. This explains any outliers in the Bland Altman plot (Figure 3.10) if both related samples are noisy in opposite directions. The calculated volume signals (Figure 3.12) are also almost perfectly congruent. As all noise is eliminated by the integration, no individual outliers can be found in the correlation plot (Figure 3.11) and in the Bland Altman plot (Figure 3.11). The good performance of the IFX-Spirometer is particularly evident in the correlation plot of the volume (Figure 3.11). The situation is similar for inhalation. Here, too, the correlation plot and the Bland

Altman plot (Figure 3.14) for the flow clearly show some outliers. For volume, the curves are again almost congruent and show this result again in the correlation plot and in the corresponding Bland Altman plot (Figure 3.15).

3.3.2.1 Exhalation

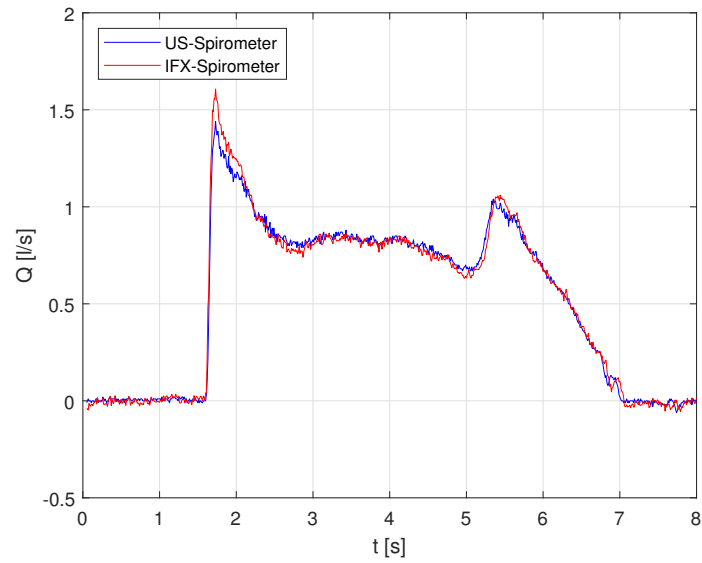


Figure 3.8: Flow of a complete exhalation measured using IFX-Spirometer (red curve) and US-Spirometer (blue curve)

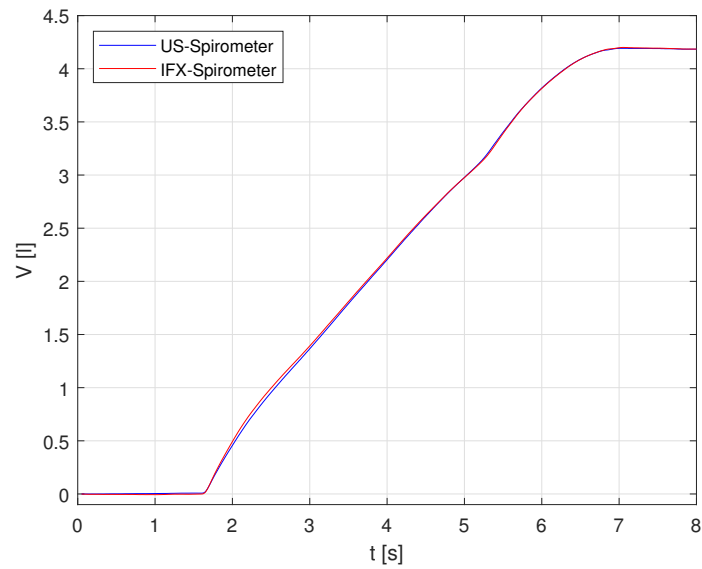


Figure 3.9: Volume of a complete exhalation measured using IFX-Spirometer (red curve) and US-Spirometer (blue curve)

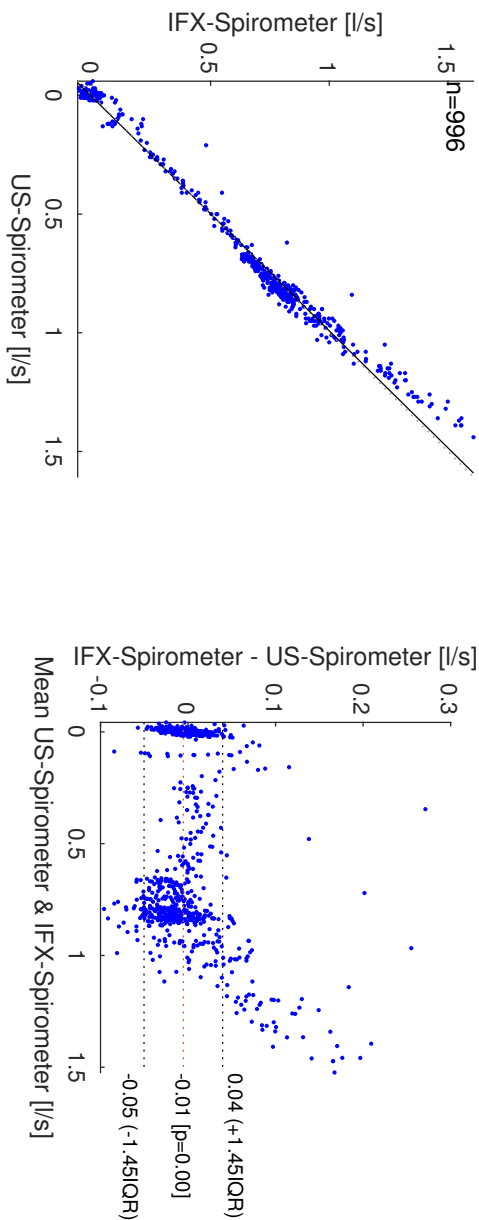


Figure 3.10: Comparison of determined Flow between IFX-Spirometer and US-Spirometer

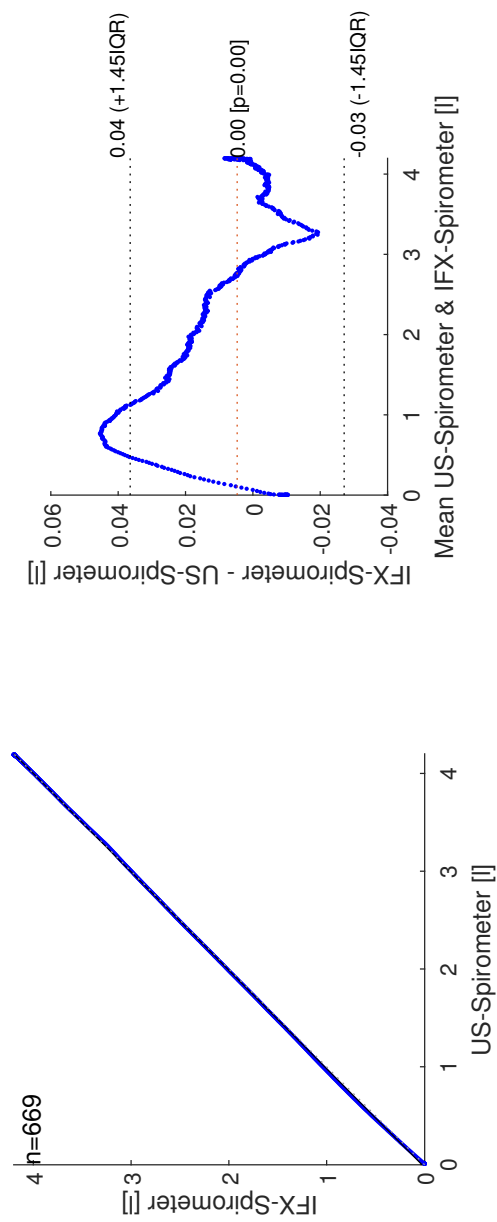


Figure 3.11: Comparison of determined volume between IFX-Spirometer and US-Spirometer

3.3.2.2 Inhalation

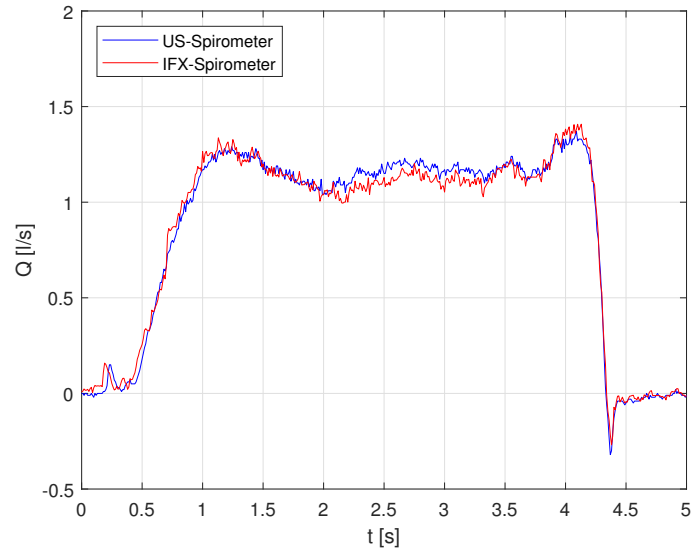


Figure 3.12: Flow of a complete inhalation measured using IFX-Spirometer (red curve) and US spirometer (blue curve)

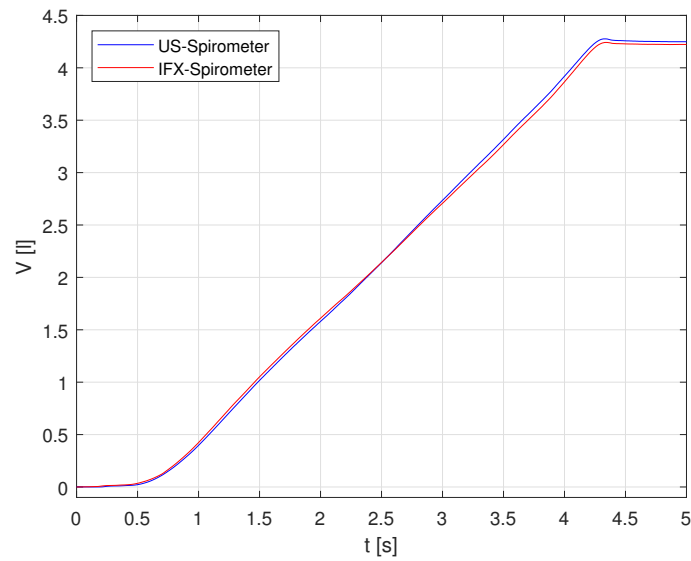


Figure 3.13: Flow of a complete inhalation measured using IFX-Spirometer (red curve) and US spirometer (blue curve)

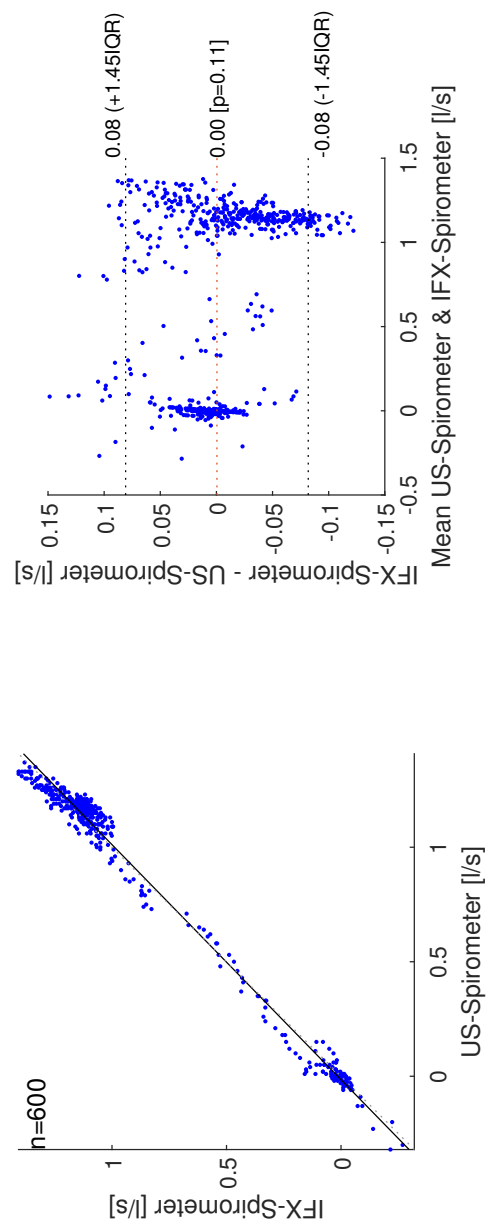


Figure 3.14: Comparison of determined volume between IFX-Spirometer and US-Spirometer

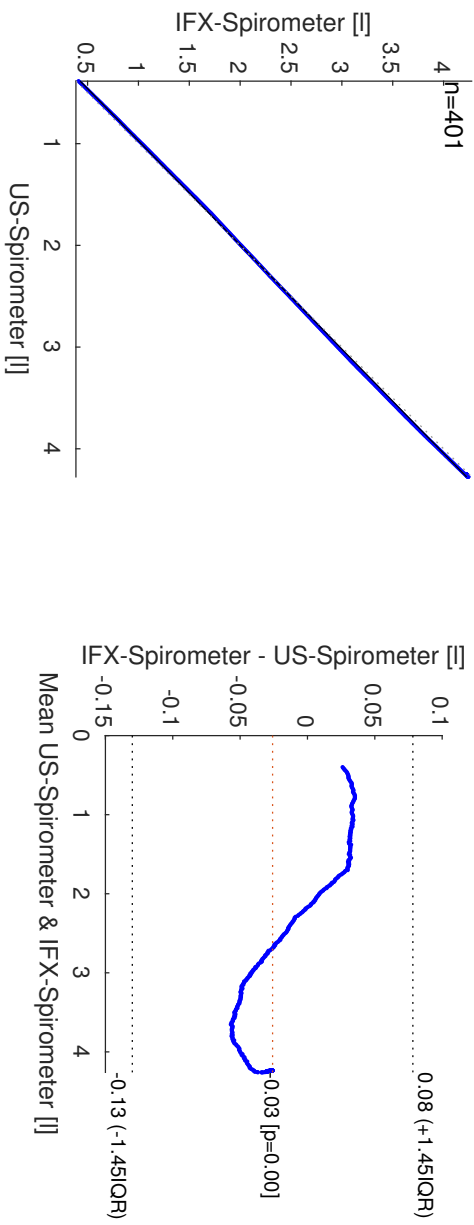


Figure 3.15: Comparison of determined volume between IFX-Spirometer and US-Spirometer

3.3.3 Charge consumption and lifetime

Results for the lifetime estimation are displayed in Figure 3.16, which shows one 5s long frame of the current consumed by the IFX-Spirometer in red. The IFX-Spirometer is connected to a central device is continuously transmitting data. The blue curve shows the consumed charge of the IFX-Spirometer during that period. Per frame the scopes calculated the maximum current peak, the average current consumption and the charge consumed, which is the maximum charge. 100 frames were recorded. In addition the scope also determines the mean, max and min of the three parameters measured per frame. For the 100 frames measured the mean current consumption of the IFX-Spirometer was 1.84 mA, with mean peak current of 44.56 mA. These peak currents are caused by the BLE radio during the transmission. The mean consumed charge of the IFX-Spirometer per frame was 9.18 mC. Using a commercially available CR2032 battery with a charge of 220 mAh, the average current consumption of 1.84 mA results in an estimated operating time of ~ 119 hours.



Figure 3.16: Screen capture of the current waveform analyzer used for the charge consumption measurement.

Discussion and Outlook

The development of a demonstrator for the measurement and wireless transmission of respiratory flow was successful. The system (IFX-Spirometer) transmits differential pressure and temperature in 24-bit values via BLE to a BLE capable host. These are processed by a MATLAB[®] script to respiratory flow and respiratory volume. The measurement accuracy in terms of flow and volume can keep pace with a state-of-the-art ultrasonic spirometer. The low power consumption results in an estimated operating time of up to 119 hours using a commercially available CR2032 battery (220 mAh charge). Most of the mechanical hardware is 3D printed and can therefore be easily replicated. The developed MATLAB[®] script allows the IFX-Spirometer to be subjected to a calibration routine. As the demonstrator is a first proof of concept, there is still room for improvement of the hardware:

- Development of a coherent system, i.e. the integration of the PCB into the flow element.
- Size reduction of PCB such as the removal of all unnecessary GPIO pins from the design, the use of smaller crystal oscillators.
- Use of a MCU with BLE 5.4, which does not require an external flash (currently not available)
- Extension of the PCB with a rechargeable battery and in-place charging circuit.

- Adding additional sensors to determine the CO_2 and O_2 value in the exhaled air.
- Adding additional sensors to determine humidity and absolute air pressure to be able to calculate BTPS conditions.

Further improvements could be implemented with regard to the relationship between differential pressure and airflow. If more information was provided by the manufacturer of the flow resistor. A professional flow generator with temperature, static pressure and humidity control could also improve the understanding of flow resistance. Furthermore, the measurement of several membranes could provide further insights, as only one membrane was characterized in the course of this work. The membrane model could also be described by a higher order polynomial, since, as can be seen in Figure 3.4, there is no ideal linear relationship between flow and differential pressure. Another point is the validity range of the model. This is only valid up to a flow of $4\frac{1}{s}$ and is therefore a long way from the required $16\frac{1}{s}$. In Figure 3.8 and Figure 3.10 one can also see that the model obviously has non-linearities in higher flow ranges. Here, the signal measured using the US-Spirometer differs significantly from the IFX-Spirometer signal.

The following further improvements to the software can be made:

- Development of an application for iOS and Android powered smartphones and tablets.
- Integration into telemedicine system for registered doctors.
- Development of an AI tool for further data processing such as pathology detection based on spirometry data.
- Implementation for over-the-air firmware updates.

Bibliography

- [1] Wikipedia. "Moore's law." (2024), [Online]. Available: https://en.wikipedia.org/wiki/Moore%27s_law (visited on 02/01/2024).
- [2] Wikipedia. "Internet of things." (2024), [Online]. Available: https://en.wikipedia.org/wiki/Internet_of_things (visited on 02/01/2024).
- [3] A. D. C. H. AG. "Eversense." (2024), [Online]. Available: <https://www.ascensiadiabetes.com/eversense/> (visited on 02/01/2024).
- [4] M. du Toit, B. Malau-Aduli, V. Vangaveti, S. Sabesan, and R. A. Ray, "Use of telehealth in the management of non-critical emergencies in rural or remote emergency departments: A systematic review," *Journal of Telemedicine and Telecare*, vol. 25, no. 1, pp. 3–16, 2019, issn: 1357-633X. doi: 10.1177/1357633x17734239.
- [5] A. Santini, A. Messina, E. Costantini, A. Protti, and M. Cecconi, "Covid-19: Dealing with ventilator shortage," *Current Opinion in Critical Care*, vol. 28, no. 6, p. 652, 2022.
- [6] R. Read. "Covid-19 ventilator projects and resources with faqs." (2022), [Online]. Available: <https://github.com/PubInv/covid19-vent-list/pulls> (visited on 08/08/2023).
- [7] W. Clauss and C. Clauss, *Humanbiologie kompakt*. Springer Berlin Heidelberg, 2018. doi: 10.1007/978-3-662-55850-8.
- [8] J. A. W. E. J. B. P. D. H. K. O. K. J. E. J. M. W. P. D. J. Gordon Betts Kelly A. Young. "Anatomy and physiology." (2013), [Online]. Available: <https://openstax.org/books/anatomy-and-physiology/pages/22-1-organs-and-structures-of-the-respiratory-system> (visited on 01/09/2025).

- [9] B. SIG. "File:lungvolumes updated.png." (2014), [Online]. Available: https://commons.wikimedia.org/wiki/File:Lungvolumes_Updated.png (visited on 01/09/2025).
- [10] R. M. S. Christian Buess and R. Kramme, *Spirometrie und erweiterte Lungenfunktionsdiagnostik*. Springer Berlin Heidelberg, 2015, pp. 1–22. doi: 10.1007/978-3-662-45538-8_13-1.
- [11] M. R. Miller, "Standardisation of spirometry," *European Respiratory Journal*, vol. 26, no. 2, pp. 319–338, 2005, issn: 0903-1936. doi: 10.1183/09031936.05.00034805.
- [12] P. Kersten, J. Wagner, P. A. Tipler, and G. Mosca, *Fluide*, 2019. doi: 10.1007/978-3-662-58281-7_10.
- [13] Wikipedia. "Bluetooth low energy." (2023), [Online]. Available: https://de.wikipedia.org/wiki/Bluetooth_Low_Energy (visited on 01/10/2023).
- [14] A. A. Circuits. "Exploring the basics of bluetooth low energy: A beginners guide to ble." (2023), [Online]. Available: <https://www.allaboutcircuits.com/technical-articles/exploring-the-basics-of-bluetooth-low-energy-a-beginners-guide-to-ble/> (visited on 01/10/2023).
- [15] Medium. "The basic concepts of bluetooth low energy (ble) for beginners." (2019), [Online]. Available: <https://pcng.medium.com/the-basic-concepts-of-bluetooth-low-energy-ble-for-beginner-c0fe062190c5> (visited on 01/10/2023).
- [16] I. Bluetooth SIG. "Bluetooth® drahtlose technologie." (2023), [Online]. Available: <https://www.allaboutcircuits.com/technical-articles/exploring-the-basics-of-bluetooth-low-energy-a-beginners-guide-to-ble/> (visited on 01/10/2023).
- [17] N. Bits. "Bluetooth low energy (ble): A complete guide." (2019), [Online]. Available: <https://novelbits.io/bluetooth-low-energy-ble-complete-guide/> (visited on 01/10/2023).
- [18] I. Bluetooth SIG. "Assigned numbers." (2024), [Online]. Available: https://www.bluetooth.com/wp-content/uploads/Files/Specification/HTML/Assigned_Numbers/out/en/Assigned_Numbers.pdf?v=1706956172775 (visited on 02/03/2024).

- [19] T. Thurner, T. Kammerhofer, B. Reiterer, and M. Hofbaur, "Tactile sensor solution with mems pressure sensors in industrial robotics," *e & i Elektrotechnik und Informationstechnik*, vol. 140, no. 6, pp. 541–550, 2023.
- [20] Infineon. "Dps368." (2019), [Online]. Available: https://www.infineon.com/dgdl/Infineon-DPS368-DataSheet-v01_01-EN.pdf?fileId=5546d46269e1c019016a0c45105d4b40 (visited on 01/03/2024).
- [21] Infineon. "Modustoolbox™ software training." (2023), [Online]. Available: <https://github.com/Infineon/training-modustoolbox-level2-btsdk/blob/master/Manual/Ch4-RTOS.pdf> (visited on 09/01/2023).
- [22] Sensirion. "Labs idea 4: Pulse monitor with differential pressure sensor." (2017), [Online]. Available: <https://developer.sensirion.com/en/archive/labs/pulse-monitor-with-differential-pressure-sensor/> (visited on 12/20/2023).
- [23] Sensirion. "Datasheet sdp3x-digital." (2022), [Online]. Available: https://sensirion.com/media/documents/4D045D69/6375F34F/DP_DS_SDP3x_digital_D1.pdf (visited on 12/20/2023).
- [24] M. Ferreira Nunes, H. Plácido da Silva, L. Raposo, and F. Rodrigues, "Design and evaluation of a novel venturi-based spirometer for home respiratory monitoring," *Sensors*, vol. 24, no. 17, p. 5622, 2024.
- [25] M. I. Research. "Spirobank ii smart." (2023), [Online]. Available: <https://www.spirometry.com/en/products/spirobank-ii-smart/> (visited on 12/15/2023).
- [26] Uscom. "Spirosonic mobile." (2023), [Online]. Available: <https://spirosonic.com/product/spirosonic-mobile-ultrasonic-spirometer/> (visited on 12/15/2023).
- [27] ndd Medizintechnik AG. "Easyone® air." (2023), [Online]. Available: <https://nddmed.com/de/produkte/spirometrie/easyone-air#downloads> (visited on 12/15/2023).
- [28] G. S. Skloot, N. T. Edwards, and P. L. Enright, "Four-year calibration stability of the easyone portable spirometer," *Respiratory care*, vol. 55, no. 7, pp. 873–877, 2010.

- [29] Infineon. “Qfn-56.” (2022), [Online]. Available: <https://www.infineon.com/cms/en/product/packages/PG-VQFN/PG-VQFN-56-809/> (visited on 12/18/2023).
- [30] Infineon. “Cyw20829.” (2022), [Online]. Available: <https://www.infineon.com/cms/en/product/wireless-connectivity/airoc-bluetooth-le-bluetooth-multiprotocol/airoc-bluetooth-le/cyw20829/> (visited on 12/18/2023).
- [31] RPubS. “Linear regression through the origin.” (2013), [Online]. Available: <https://rpubs.com/aaronsc32/regression-through-the-origin> (visited on 08/15/2023).
- [32] T. M. Inc., *Matlab version: 9.12.7 (r2022a)*, Natick, Massachusetts, United States, 2024. [Online]. Available: <https://www.mathworks.com>.
- [33] Infineon. “Modustoolbox™ software.” (2023), [Online]. Available: <https://www.infineon.com/cms/de/design-support/tools/sdk/modustoolbox-software/> (visited on 12/10/2023).
- [34] FreeRTOS. “Freertos™.” (2023), [Online]. Available: <https://www.freertos.org/index.html> (visited on 09/01/2023).
- [35] Mathworks. “Trapezoidal numerical integration.” (2013), [Online]. Available: <https://de.mathworks.com/help/matlab/ref/trapz.html> (visited on 01/15/2023).
- [36] B. Fornberg, “Improving the accuracy of the trapezoidal rule,” *SIAM Review*, vol. 63, no. 1, pp. 167–180, 2021.

APPENDIX **A**

**Instruments and assembly
equipment**

The following table A.1 contains all measurement instruments and assembly equipment used in the course of this work.

Device type	Model	Manufacturer
Evaluation Kit	CYW920829EVK-02	Infineon Technologies
USB-IIC/SPI Interface	USB 8452	National Instruments
TRMS Multimeter	85 III	Fluke
Axial fan	8212 JH4	EBM Papst
1 GHz Mixed Signal Oscilloscope	Waverunner 9104-MS	Teledyne LeCroy
Current Waveform Analyzer	CX3324A	Keysight
Triple Output DC Power Supply	E36313A	Keysight
Microscope	Lynx	Evo
Rework Station	Ersa	Hybrid Rework 550
Pick & Place machine	LM901	Fritsch
Stencil Printer	SD 903.005	Fritsch
Soldering Station	CD-2BQF	JBC Tools
3D-Printer	2+Connect	Ultimaker
Ultrasound Spirometer	Easy on-PC Spirometer	ndd

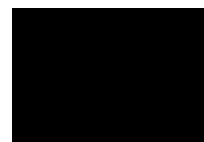
Table A.1: Used equipment for assembly and testing

The following table A.2 contains all components needed to build the IFX-Spirometer.

Device	Quantity	Manufacturer
CYW20829	1	Infineon Technologies
DDPS	1	Infineon Technologies
QSPI Flash	1	GigaDevice
Bandpassfilter 0402 2.45 GHz	1	Würth Elektronik
SMD Antenna	1	Molex
Crystal 32.768 kHz	1	TXC
Crystal 24 MHz	1	Epson
Capacitor 0402 4.7 μ F	1	TDK
Capacitor 0402 2.2 μ F	1	TDK
Capacitor 0402 1 μ F	6	TDK
Capacitor 0402 10 μ F	1	TDK
Capacitor 0402 9 pF	2	TDK
Capacitor 0402 12 pF	2	TDK
Capacitor 0201 8.2 pF	2	TDK
Capacitor 0201 100 nF	16	TDK
Capacitor 0201 10 pF	1	TDK
Capacitor 0402 1 μ F	1	TDK
Resistor 0201 10 k Ω	11	Vishay
Resistor 0402 10 M Ω	1	Vishay
Ferrite 0402 600R @10MHz	3	Murata
Pin header 2.54mm	34	Harwin
Push Button	1	Panasonic
Pneumatic connection 4 M4	4	Spore
Spirometer membrane	1	Schiller
3D printed chamber	2	Infineon Technologies
3D printed flow element	2	Infineon Technologies
Pulmo-Protect filter	1	Habel Medizintechnik

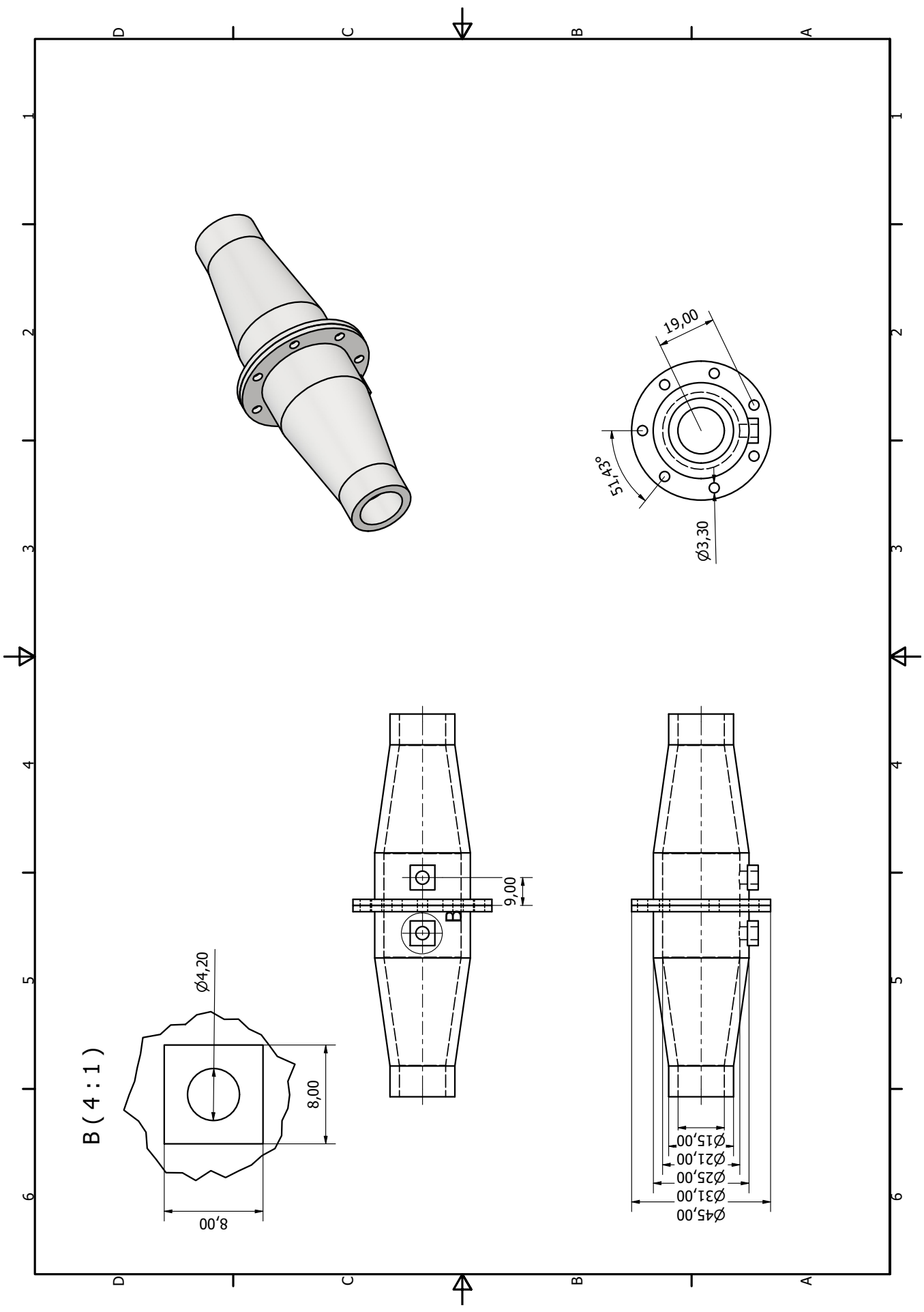
Table A.2: List of materials necessary for assembling a single module V1.0

APPENDIX **B**

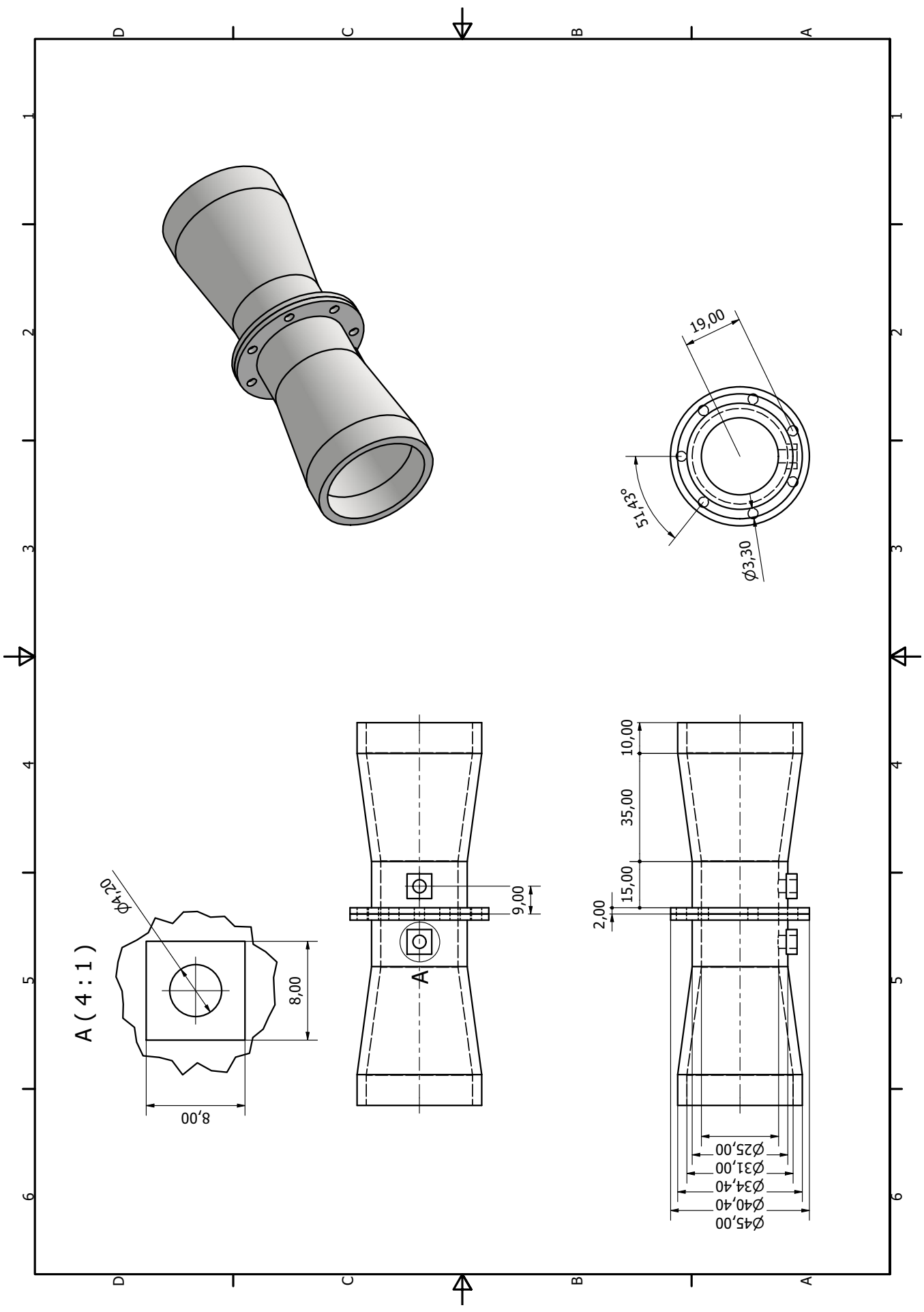


Inventor

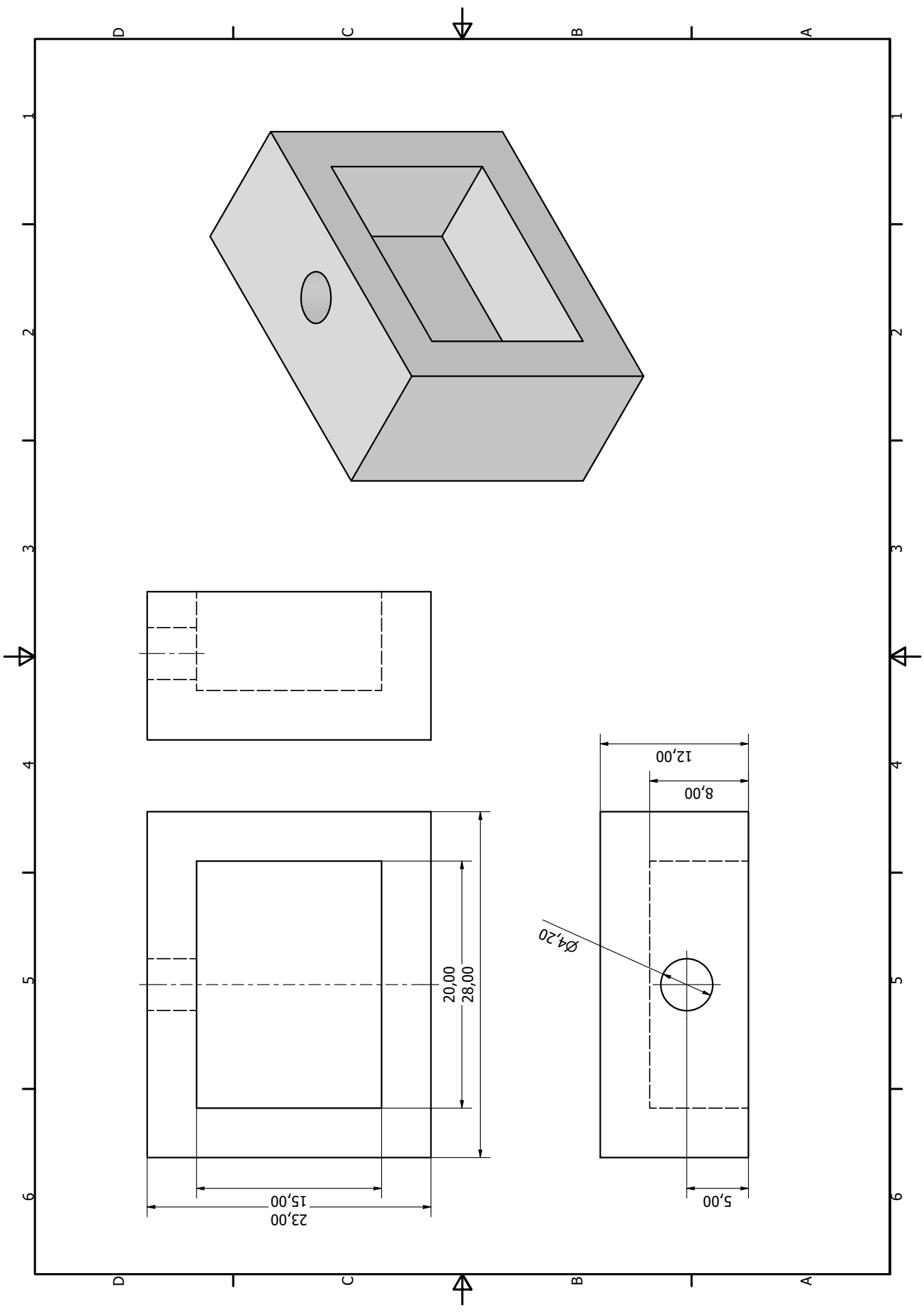
B.1 Flowelement V1



B.2 Flowelement V2



B.3 Pressure Chamber



Printed Circuit Boards

C.1 Sensor PCB V2

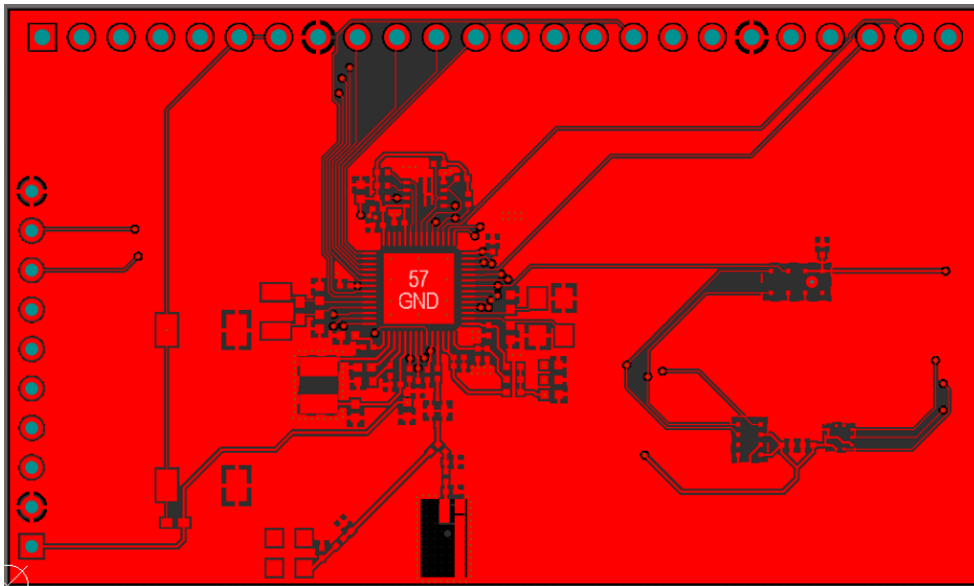


Figure C.1: Top layer of the Sensor PCB V2

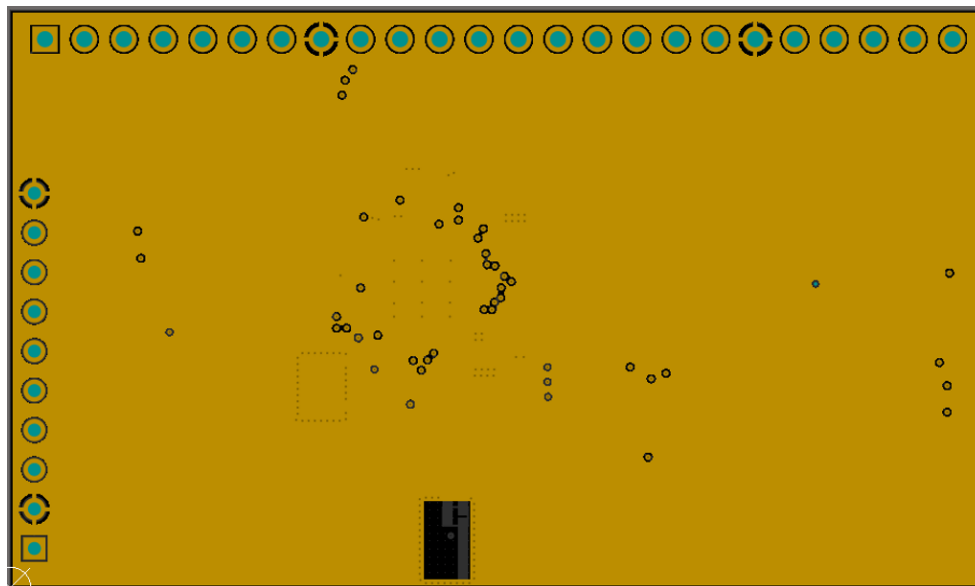


Figure C.2: Layer 2 of the Sensor PCB V2

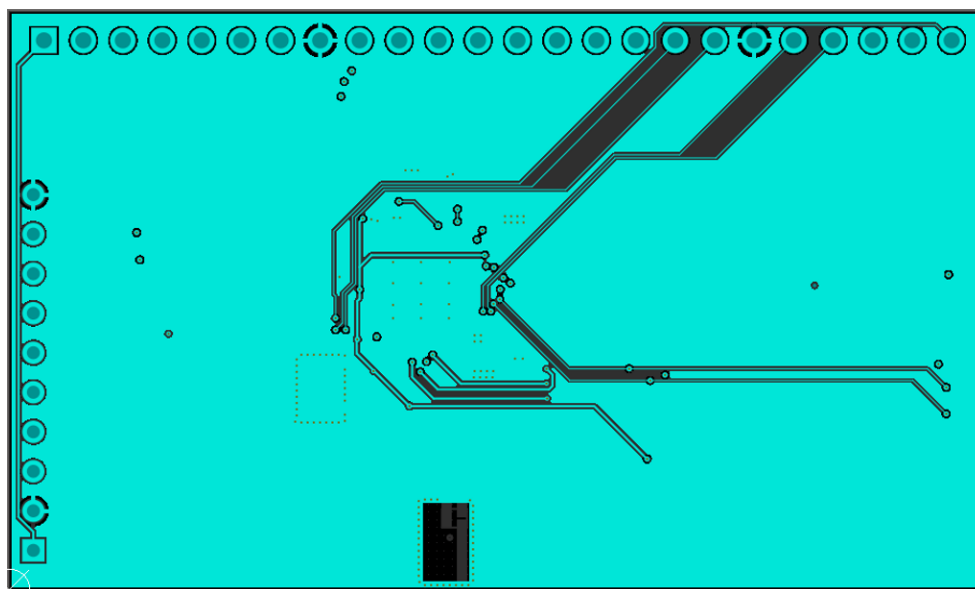


Figure C.3: Layer 3 of the Sensor PCB V2

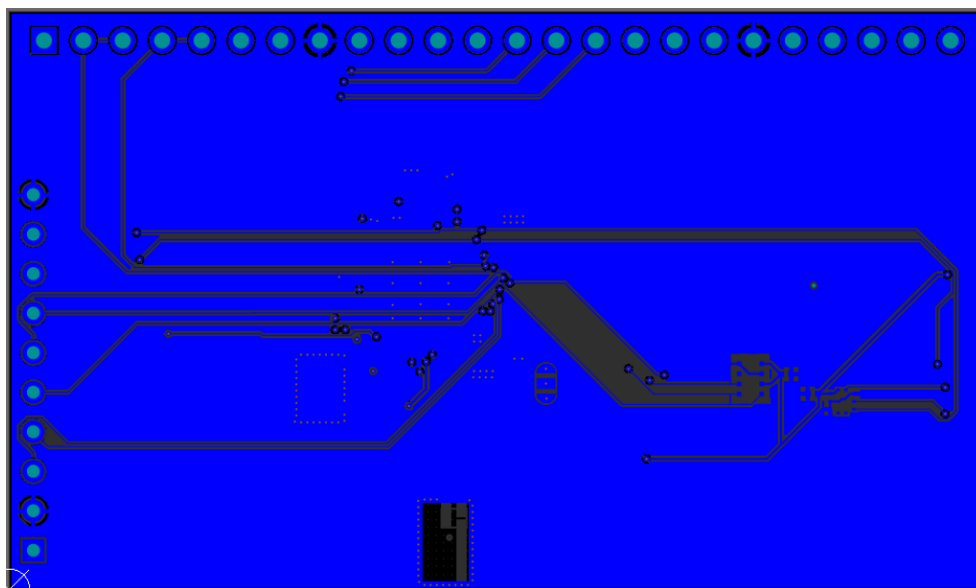


Figure C.4: Bottom layer of the Sensor PCB V2